# Interacting bound states in the continuum in Fabry-Pérot resonators: Merging, crossing, and avoided crossing

N. M. Shubin ●, V. V. Kapaev ●, and A. A. Gorbatsevich ●

*P.N. Lebedev Physical Institute of the Russian Academy of Sciences, 119991 Moscow, Russia*

We study both analytically and numerically the interaction between bound states in the continuum (BICs) in 2D Fabry-Pérot (FP) resonators in waveguides with waveguide expansions playing the role of the "mirrors." The derived analytical model illustratively captures recently proposed twin-BICs (TBICs) stemmed from BICs in individual mirrors as well as the well-known FP BICs related to an FP resonance. We show that the formation of TBICs is a universal phenomenon, which occurs in different types of FP resonators, and is related to the sharp dependence of the phase of mirror reflection coefficient on system parameters near the BIC point in the parameter space of individual mirror. We also show explicitly that the complicated multimode interference taking place in the mirrors resulting in the coalescence of two perfect transmission Fano antiresonances can explain the merging of corresponding FP BICs without invoking topological concepts. Moreover, the coalescence of antiresonances in an individual mirror can be continuously changed into the crossing or even the avoided crossing (repulsion) of antiresonances by an infinitesimal change of parameter. The behavior of FP BICs follows the antiresonances pretty closely and demonstrates a similar transformation (either merging or repulsion, respectively). The results of the analytical model are confirmed by numerical simulations of quantum-mechanical and optical waveguides.

## I. INTRODUCTION

A novel approach to create high-$Q$ resonances has been developed in past years [1–4]. This approach is based on the use of bound states in the continuum (BICs), which is a widespread wave phenomena studied both theoretically and experimentally in different branches of optics, quantum mechanics, atomic physics, electrodynamics, acoustics, and hydrodynamics (see the reviews [5–10]). BICs are localized states with the energies (frequencies) lying within the continuum of propagating states (above the light cone in optics). They are also known as states embedded in the continuum [7]. Decoupling of BIC from the continuum can result from different physical mechanisms [5–10]. Commonly one distinguishes symmetry protected (SP) BICs—decoupling due to different symmetries of propagating and localized states, Friedrich-Wintgen (FW) [11], and Fabry-Pérot (FP) [5,12] mechanisms. Also, the so-called accidental BICs may appear in consideration, which, in general, do not fit unambiguously to one of the aforementioned models [13–15].

FW BIC originates from destructive interference of waves scattered by two resonant states [11]. Hence it is closely related to another common wave phenomena—Fano resonance [16], whose transmission minimum (antiresonance) is also caused by destructive interference. The formation of FW BIC is often interpreted as a collapse of the Fano resonance with its antiresonance width turning to zero [17–19]. On the other hand, for the same reason, BIC can be considered as a collapse of the resonance (transparency maximum) with the resonance width going to zero as well [7,19]. The Fano resonance is also responsible for FP BIC. There it determines the opaqueness of the structures, which play the role of a perfect mirrors forming FP cavity, where a wave is trapped. FP BIC also can be attributed to a special kind of FW BIC [10] with one of the

two FW resonances being the Fano resonance and the other the cavity resonance. At the very energy (frequency) of FP BIC, the transmission coefficient equals zero. However, the transparency of FW BIC can possess in general any physically valid value depending on the ratio of the system parameters ensuring the formation of the resonance or antiresonance [19,20].

A separate type is constituted by BICs representing a loss-less guided mode above the light cone in infinite periodic photonic structures: 1D (e.g., chains of dielectric spheres or disks) [21–23] and 2D (e.g., gratings, metasurfaces, and photonic crystal slabs) [2,13,24–26]. Such a mode originates from a leaky resonance and decouples from the continuum through similar mechanisms as finite size BICs (SP, FW or accidental parameter tuning) [5,10]. 2D guided mode BIC manifests itself by the polarization singularity in the Bloch quasimomentum plane [14,27]. Under the variation of system parameters, this point moves in the momentum plane but persists, which highlights its topological nature, and hence, a topological protection of such BICs [14]. In Ref. [14], it was shown that BICs in 2D photonic slabs, indeed, possess a quantized topological charge, defined by the winding number of electrical field polarization, and behave as topologically charged quasiparticles: BICs with the same charges repel and with opposite charges annihilate. In Refs. [23,28], topological charges were introduced also for 1D chains of rods and spheres. These results show that BICs in some cases can be considered as particlelike objects possessing topological charges. Recently an analogy between BICs and particlelike objects was extended to the case of interacting BICs in the FP structures, where twin-BICs (TBICs) were described [29], which can be considered as tunneling coupled BICs of individual mirrors of the FP resonator. FP BICs exist in a wide

range of the mirror parameters, which preserves the Fano antiresonance, and for a discrete set of cavity lengths that provide a phase matching condition. In contrast, TBICs are almost independent on the cavity length and exist in a narrow range of mirror parameters, where BIC in individual mirror arise. Thus FP BICs and TBICs can be considered complementary to each other.

The quality factor ($Q$-factor) is determined by the relation of stored and radiated (outgoing) energies. It can be measured as a ratio of central frequency to the resonance width. Formally, BIC possesses an infinite $Q$-factor. In the energy-parameter space, BIC, typically, corresponds to a single point. Thus BIC formation conditions can hardly be met exactly in practice. In the nearby vicinity of BIC point, it turns into an extremely narrow resonance (quasi-BIC). If we denote by $\Delta p$ the deviation of some parameter $p$ from the exact value corresponding to BIC formation $p_{\text{BIC}}$, then, in general, the $Q$-factor of the quasi-BIC resonance is proportional to $\Delta p^{-2}$ [2,11]. Recently, a great interest arose in the discovery that near some points in the parameter space of 2D guided mode BIC, $Q$-factor blows up as $\Delta p^{-n}$ with $n > 2$ [26,30,31] (supercavity BIC or super-BIC in Ref. [26]). Such points correspond to merging of topological BICs in momentum space. In Ref. [26], merging of SP and accidental BICs was experimentally achieved and performance of ultralow-threshold laser with a small footprint was demonstrated. Therefore studying interaction of BICs provides a regular way to constructing structures with ultrahigh-$Q$ resonances for a wide range of applications.

Guided mode BICs in realistic finite structures turn into quasi-BICs with the large but finite $Q$-factor [26,32,33]. Another example of finite structures possessing BICs are resonators within waveguide [34–37]. Recently, the merging of FW [36] and FP [37] BICs in finite resonators has been described and interpreted in terms of annihilation of opposite topological charges. An essential difference between the BIC topological description in finite (resonators) and infinite (slabs) systems is that in the latter case, it is formulated in terms of quasimomentum components, which are directly related to the observable polarization of electromagnetic field [14,27,30,31]. The closed curve around a given BIC point describes the evolution of polarization in a given system, which can be measured in the far zone. Contrary, analogous contour around the BIC point in the parameter space of a finite system is formed by an infinite continuous set of points each corresponding to different system (with different values of the parameters) that is obviously hardly observable. Consequently, a natural and important question arises, whether topological properties of BICs in finite systems are fundamental or emergent, and interaction of BICs can be described without involving ideas about their topological nature. We partially address this question in our paper by studying interacting FP BICs in 2D FP waveguide structure both by analytical consideration and numerical modeling. The peculiarity of the system is that mirrors comprising FP resonators exhibit complicated transformations of resonances and antiresonances in the parameter space thus affecting BIC formation condition for the whole FP structure. In particular, we show that Fano resonances in mirrors can coalesce and destroy FP BICs. Such a behavior is analogous to annihilation

of BICs with opposite topological charges but surely is of quite different physical origin.

The structure of our paper is as follows. In Sec. II, the quantum-mechanical eigenvalue problem for finding BICs in multimode FP resonators is formulated and solved analytically within the two-mode approximation. The analysis of the proposed two-mode quantum-mechanical model provides a comprehensive description of FP BICs, TBICs, and their mutual interaction. In Sec. III, we describe topological-like [37] merging of FP BICs due to a nontopological phenomenon of the antiresonance coalescence in individual mirrors [19,38]. Moreover, the continuous transition in the parameter space can be observed between merging and repulsion of FP BICs. Additionally, in Sec. III, we show that the $Q$-factor grows in proportion to $\Delta p^{-4}$ in the avoided crossing region. Hence, BIC merging is not a necessary condition for such growth. Section IV is devoted to numerical simulations of 2D quantum-mechanical and optical waveguides that confirm main results of the analytical consideration. Finally, conclusions are made in Sec. V.

## II. ANALYTICAL MODEL OF BOUND STATES IN THE CONTINUUM IN FABRY-PÉROT RESONATORS

### A. Quantum-mechanical multimode model

We consider a two-dimensional waveguide along the $x$ axis with two identical resonators (confinement regions) of length $L$ located at a distance $D$ from each other (see Fig. 1). These resonators play the role of mirrors, which can trap the wave in the resulting FP cavity between them. In the simplest single-mode case (without taking into account evanescent modes in the cavity), the transmission coefficient of an FP resonator takes the form [39]

$$T_{\text{FP}} = \frac{T^2}{1 + R^2 - 2R \cos{(2kD + 2\varphi)}}, \qquad (1)$$

where $kD = 2\pi D/\lambda$ is the phase acquired by the wave traveling between the mirrors, $\varphi$ is the phase of the complex reflection amplitude of the mirror, $R = 1 - T$ is the reflection coefficient, and

$$T = \frac{|P|^2}{|P|^2 + |Q|^2} \qquad (2)$$

is the transmission coefficient of the mirror [19,35]. Such a type of structures is known for the formation of Fano resonances with complicated behavior [40–42].

Functions $P$ and $Q$ in Eq. (2) are analytical functions of energy (frequency), which are determined by the specific structure of the resonator playing role of a mirror. At the energy providing $P = Q = 0$, BIC in a single isolated resonator is formed [19,35]. Similarly, BIC in the whole FP structure corresponds to simultaneous turning to zero of the numerator and denominator in Eq. (1). Thus, from Eqs. (1) and (2), it follows straightforwardly that conditions

$$P = 0,$$
$$D = \left(n - \frac{\varphi}{\pi}\right)\frac{\lambda}{2}, \quad n \in \mathbb{N}. \qquad (3)$$

provide perfect wave trapping in the FP cavity. The first equation in (3) is related to the antiresonance of a single mirror
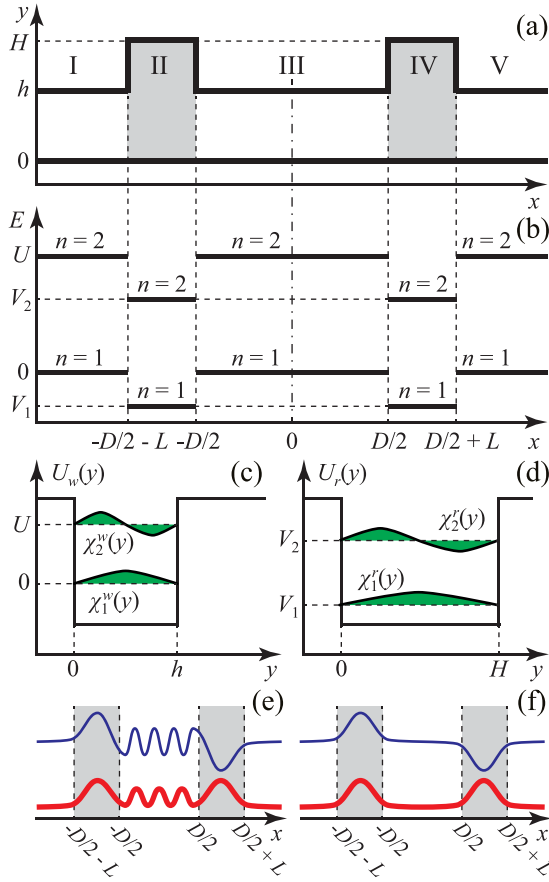
FIG. 1. (a) Schematic view of 2D waveguide with two equal resonators shown by gray and (b) corresponding spatial distribution of the first two transverse mode thresholds. Resonators are depicted as waveguide expansions. However, they can be designed in any other manner, e.g., by additional attractive potential. Notation corresponds to Sec. II B. (c) Illustration of transverse modes inside the waveguide and (d) inside the resonator. [(e) and (f)] Schematic view of the longitudinal wave-function distribution for symmetric (red thick line) and antisymmetric (blue thin line) FP BICs (e) and TBICs (f).

since it provides $T = 0$. For $P \neq 0$, the second relation in (3) describes typical FP resonance with $T_{FP} = 1$. It can be shown that together both BIC conditions (3) correspond to $T_{FP} = 0$ (incident wave is perfectly reflected from the first mirror).

In waveguide structures, multimode interference do play a role (see, e.g., Refs. [17,35,42,43]), resulting in a complicated behavior of the reflection coefficient $R$ and phase $\varphi$ that gives rise to a rich variety of different BIC related phenomena. In the considered two-resonator structure, we assume that the potential energy $U(x, y)$ is a piecewise constant function of $x$. In particular, we set $U(x, y) = U_w(y)$ in waveguides (regions I, III, and V in Fig. 1) and $U(x, y) = U_r(y)$ in resonators (regions II and IV in Fig. 1). The solution to the two-dimensional stationary Schröedinger equation

$$\frac{\partial^2 \Psi}{\partial x^2} + \frac{\partial^2 \Psi}{\partial y^2} + [E - U(x, y)]\Psi = 0 \qquad (4)$$

for either scattering or eigenvalue problem can be constructed, e.g., by the transverse modes decomposition method [44–47].

In Eq. (4), we have set the mass of the particle to be a constant and have chosen the units such that $\frac{\hbar^2}{2m} = 1$.

Within each region, one can separate variables and look for the solution of Eq. (4) in the form $\Psi_j(x, y) = \sum_n \psi_n^j(x)\chi_n^j(y)$ [44–47], where $j$ is the region number ($j = 1, 3, 5$ in the waveguides and $j = 2, 4$ in the resonators) and $n$ enumerates transverse modes derived from the equation

$$\frac{\partial^2 \chi_n^j(y)}{\partial y^2} + [\xi_n^j - U_j(y)]\chi_n^j(y) = 0, \qquad (5)$$

where $U_j(y) = U_w(y)$ for $j = 1, 3, 5$ and $U_j(y) = U_r(y)$ for $j = 2, 4$ [see, e.g., Figs. 1(c) and 1(d)]. Here $\xi_n^j$ is the separation constant, which is treated as a threshold of the $n$th transverse mode in the $j$th region and plays the role of potential energy in the equation for longitudinal function $\psi_n^j(x)$:

$$\frac{\partial^2 \psi_n^j(x)}{\partial x^2} + (E - \xi_n^j)\psi_n^j(x) = 0. \qquad (6)$$

From this equation, one can see that within each region potential energy for longitudinal wave functions is constant, and hence $\psi_n^j(x)$ can be written as a superposition of left- and right-going plane waves with wave vectors $k_n^j = \sqrt{E - \xi_n^j}$.

Matching wave functions $\Psi_j(x, y)$ and their derivatives, one can formulate the continuity condition for the longitudinal components at the border between the $j$th and the $(j + 1)$th regions as

$$\psi_n^{j+1}(x_j) = \sum_m (\hat{\mu}_j)_{mn}\psi_m^j(x_j),$$

$$\frac{\partial \psi_n^{j+1}(x_j)}{\partial x} = \sum_m (\hat{\mu}_j)_{mn}\frac{\partial \psi_m^j(x_j)}{\partial x}. \qquad (7)$$

Here $\hat{\mu}_j$ is a unitary infinite-dimensional transformation matrix between basis sets $\{\chi_m^j\}$ and $\{\chi_m^{j+1}\}$. For the symmetric structure under consideration, we have $\hat{\mu}_1 = \hat{\mu}_3 = \hat{\mu}$ and $\hat{\mu}_2 = \hat{\mu}_4 = \hat{\mu}^\dagger$ with matrix elements being

$$\mu_{mn} = \int_{-\infty}^{\infty} \chi_m^w(y)\chi_n^{r*}(y)dy. \qquad (8)$$

Matrix elements (8) are real for localized transverse eigenfunctions $\chi_n^{r,w}$ given by solutions of Eq. (5) with discrete spectrum.

BIC with energy $E_{BIC}$ in the considered structure must have a zero amplitude of outgoing waves in all propagating (open) modes in the first and fifth regions (i.e., for all $i$ providing $E_{BIC} \geqslant \xi_i^{1,5}$). In the present paper, we focus on a case with a single propagating mode in the waveguide, so we restrict ourselves to the energy range $\xi_1^{1,5} < E < \xi_2^{1,5}$.

### B. Two-mode approximation

The exact solution of the Schröedinger equation (4) by the transverse mode decomposition method requires the infinite number of modes to be taken into account (including both discrete and continuous spectrum in the $y$ direction). However, some features of BICs formation and their behavior can be captured within finite-mode approximations [35,43]. In this section, we restrict ourselves to a two-mode approximation

with the following mode thresholds: $\xi_1^1 = \xi_1^3 = \xi_1^5 = 0$, $\xi_2^1 = \xi_2^3 = \xi_2^5 = U$, $\xi_1^2 = \xi_1^4 = V_1$, and $\xi_2^2 = \xi_2^4 = V_2$ (see Fig. 1). The mode coupling matrix $\mu$ in this case is $2 \times 2$ orthogonal matrix:

$$\hat{\mu} = \begin{pmatrix} \cos\theta & \sin\theta \\ -\sin\theta & \cos\theta \end{pmatrix}, \qquad (9)$$

where $\theta \in \mathbb{R}$ defines the mode mixing at a waveguide/resonator interface. Analytical solution to a scattering problem through the considered structure is quite cumbersome and can hardly provide physical insight into BIC formation mechanism (even within the two-mode approximation), whereas eigenvalue problem for finding BIC can be solved and interpreted illustratively.

The structure under consideration is invariant under reflection $x \mapsto -x$. Hence, solutions to the eigenvalue problem (4) are either symmetric or antisymmetric. Within the two-mode model, we have the following ansatz for the longitudinal wave function of BIC in the outer region: $\psi_1^1(x) = \psi_1^5(x) \equiv 0$. Then, we have

$$\psi_2^1(x) = \sigma_p \psi_2^5(x) = a_2^p e^{-\kappa(|x| - \frac{D}{2} - L)}, \qquad (10)$$

outside the resonator and

$$\psi_{1,2}^2(x) = \sigma_p \psi_{1,2}^4(x) = c_{1,2}^p \cos\left[q_{1,2}\left(|x| - \tfrac{D+L}{2}\right) + \alpha_1^p\right], \qquad (11)$$

inside the mirrors, where $p \in \{s, a\}$ indicates the parity of the state with respect to $x \mapsto -x$ reflection ($s$–symmetric, $a$–antisymmetric) and $\sigma_s = -\sigma_a = 1$. Finally, in the central region between the mirrors, we set

$$\psi_1^3(x) = b_1^s \cos kx \quad \text{and} \quad \psi_2^3(x) = b_2^s \cosh \kappa x \qquad (12)$$

in the symmetric case or

$$\psi_1^3(x) = b_1^a \sin kx \quad \text{and} \quad \psi_2^3(x) = b_2^a \sinh \kappa x \qquad (13)$$

in the antisymmetric case. Here $k = \sqrt{E}$, $\kappa = \sqrt{U - E}$, and $q_{1,2} = \sqrt{E - V_{1,2}}$. Applying matching conditions (7) to these solutions, one gets a system of eight equations for seven unknowns $a_2^s$, $b_{1,2}^s$, $c_{1,2}^s$, and $\alpha_{1,2}^s$ for symmetric BIC and $a_2^a$, $b_{1,2}^a$, $c_{1,2}^a$, and $\alpha_{1,2}^a$ for antisymmetric BIC. The consistency condition of this system of equations provides BIC energy and required structure parameters. On the other hand, these equations can be considered as a linear homogeneous system for five amplitudes. In this case, consistency conditions are straightforward:

$$\tan\left(\frac{q_{1,2}L}{2} + \alpha_{1,2}^p\right) = \frac{\kappa}{q_{1,2}},$$
$$\tan\left(\frac{q_1 L}{2} - \alpha_1^p\right) = \frac{\kappa' - \Delta\kappa}{q_1},$$
$$\tan\left(\frac{q_2 L}{2} - \alpha_2^p\right) = \frac{\kappa' + \Delta\kappa}{q_2}, \qquad (14)$$

where

$$\kappa' = \kappa\left[1 - \frac{f_p}{2}(1 - \eta\cos^2\theta - \eta^{-1}\sin^2\theta)\right.$$
$$\left. - \frac{g_p}{2}(1 + \eta\cos^2\theta + \eta^{-1}\sin^2\theta)\right] \qquad (15)$$

and

$$\Delta\kappa = \frac{\kappa}{2}[f_p(\cos 2\theta + \eta^{-1}\sin^2\theta - \eta\cos^2\theta)$$
$$+ g_p(-\cos 2\theta + \eta\cos^2\theta - \eta^{-1}\sin^2\theta)]. \qquad (16)$$

Here we have also introduced $f_s = 1 + \frac{k}{\kappa}\tan(kD/2)$, $f_a = 1 - \frac{k}{\kappa}\cot(kD/2)$, $g_s = 1 - \tanh(\kappa D/2)$, $g_a = 1 - \coth(\kappa D/2)$ and

$$\eta = \frac{q_1}{q_2} \times \frac{q_2\cos q_2 L + \kappa\sin q_2 L}{q_1\cos q_1 L + \kappa\sin q_1 L}. \qquad (17)$$

The first equation (in fact, two equations: with $q_1$, $\alpha_1^p$ and $q_2$, $\alpha_2^p$) in the system (14) corresponds to the border at $x = \pm(D/2 + L)$ between the mirrors and the outer waveguides, where the wave function of BIC is present in the second transverse mode only. For $\alpha_{1,2}^s = 0$ and $\alpha_{1,2}^a = \frac{\pi}{2}$ it becomes similar to the case of a single symmetric potential well with bottom energy $V_{1,2}$ and barrier height $U$ [42]. If $\alpha_{1,2}^p \neq 0, \frac{\pi}{2}$, then the first equation corresponds to the asymmetric potential well (see Appendix A). Considering the border at $x = \pm D/2$ between the mirrors and the inner waveguide, one gets the rest equations in (14). Neglecting $\Delta\kappa$, these equations again give the case of a single asymmetric potential well (Appendix A). In the considered system, effective asymmetry of the locally symmetric mirror arises due to the presence of another mirror, which makes waveguides to the left and to the right of the mirror to be nonequivalent. However, this asymmetry is more complicated compared to the asymmetric potential well discussed in Appendix A because it differently affects different modes with $\Delta\kappa \neq 0$ in general.

Equations (14) define phases $\alpha_{1,2}^p$, energies and structure parameters (e.g., $D$ or $L$) of BICs. One can eliminate phases from these equations and get the following nonlinear system for BIC energy and structural parameters:

$$P = -\sigma_{s,a}kZ_+ e^{-\kappa D},$$
$$B\sin\left(\frac{kD}{2} + \varphi_{s,a}\right) = 0. \qquad (18)$$

Here $P$ is the numerator of the individual resonator transmission coefficient (2). In our two-mode model, $P$ is given by [35]

$$P = 2k(q_1 S_{222}A_{222}\cos^2\theta + q_2 S_{212}A_{212}\sin^2\theta) \qquad (19)$$

with

$$S_{2n2} = q_n\sin\left(\frac{q_n L}{2}\right) - \kappa\cos\left(\frac{q_n L}{2}\right),$$
$$A_{2n2} = \kappa\sin\left(\frac{q_n L}{2}\right) + q_n\cos\left(\frac{q_n L}{2}\right). \qquad (20)$$

Quantities $S_{2n2}$ and $A_{2n2}$ (more precisely, the equations $S_{2n2} = 0$ and $A_{2n2} = 0$) define symmetric ($S$) and antisymmetric ($A$) states 2-$n$-2 of a single resonator embedded into the waveguide. State 2-$n$-2 is localized at the $n$th transverse mode inside the resonator and decays exponentially at the second (evanescent) mode in waveguide [35,43]. In the second equation in (18), we have introduced

$$B = \sqrt{(Z_0 - \sigma_{s,a}Z_-)^2 + \left(\frac{\kappa}{k}\right)^{2\sigma_{s,a}}(Z_0 + \sigma_{s,a}Z_-)^2} \qquad (21)$$

and

$$\varphi_s = \frac{\varphi}{2}, \quad \varphi_a = \frac{\varphi}{2} + \frac{\pi}{2} \tag{22}$$

with

$$\varphi = 2\arctan\left(\frac{\kappa}{k} \times \frac{Z_- + Z_0}{Z_- - Z_0}\right), \tag{23}$$

being the phase of the reflection coefficient of the individual resonator under the condition of perfect reflection ($P = 0$). The rest quantities in Eqs. (18) and (23) are the following:

$$\begin{aligned} Z_+ &= q_1(U - V_2)\sin q_2 L \cos^2\theta \\ &\quad + q_2(U - V_1)\sin q_1 L \sin^2\theta, \\ Z_0 &= 2(q_1 S_{222} A_{222} - q_2 S_{212} A_{212}), \\ Z_- &= q_1(U - V_2)\sin q_2 L - q_2(U - V_1)\sin q_1 L. \end{aligned} \tag{24}$$

BIC formation condition (18) represents the main result of the analytical consideration within the two-mode approximation.

### C. Fabry-Pérot and twin bound states in the continuum in two-mode model

In the simple $\delta$-functional model proposed in Ref. [29], FP BICs and TBICs were independent solutions of the corresponding multimode eigenvalue problem. In the present paper, finite length of the mirrors leads to the hybridization of these two types of BICs due to evanescent coupling between the mirrors. Therefore, at first, it is illustrative to interpret the system (18) for mirrors located far from each other such that $\kappa D \gg 1$ and one can neglect the evanescent coupling in the energy range of interest. In this case, the first equation becomes identical to the result of the trivial single-mode consideration (3), and hence BIC energy $E_{\text{BIC}}$ and corresponding length $L_{\text{BIC}}$ are directly related to the antiresonances ($P = 0$) of the individual mirror [19,35]. Under this assumption, the fulfillment of the second equation in (18) can take place either for $\sin(kD/2 + \varphi_{s,a}) = 0$ or for $B = 0$ similarly to the model in Ref. [29]. In the former case, the second equation can be rewritten as in the single-mode model (3) with $\varphi$ given by Eq. (23), which describes the buildup of the FP resonance. Even $n$ in the second equation in system (3) corresponds to symmetric (with respect to $x \mapsto -x$) and odd $n$—to antisymmetric solutions. Described BICs are of the Fabry-Pérot type [Fig. 1(e)] with strictly nonzero wavefunction amplitudes $b_1^{s,a}$ inside the FP cavity [see Eqs. (12) and (13)]:

$$\begin{aligned} b_1^{s,a} &\propto c_1^{s,a}[q_2(q_1 \cos q_1 L + \kappa \sin q_1 L) \\ &\quad - q_1(q_2 \cos q_2 L + \kappa \sin q_2 L)], \end{aligned} \tag{25}$$

where $c_1^{s,a}$ is the wave-function amplitude at the first mode inside the mirrors, which we assume to be nonzero.

The case $B = 0$ corresponds to the recently proposed new type of BICs [29]. These BICs are related to BICs in individual mirrors rather than to the FP resonance between them. They were called twin-BICs (TBICs) as they appear in pairs—symmetric and antisymmetric ones [Fig. 1(f)]. According to Eq. (21), condition $B = 0$ implies $Z_0 = 0$ and $Z_- = 0$ simultaneously. From Eqs. (24), it can be shown that this is fulfilled by

$$S_{222} = 0, \quad S_{212} = 0, \tag{26}$$

for symmetric TBIC or by

$$A_{222} = 0, \quad A_{212} = 0 \tag{27}$$

for antisymmetric TBIC. Conditions (26) and (27) correspond to symmetric and antisymmetric BICs in isolated mirrors [35], respectively. Moreover, these conditions also provide $P = 0$ [see Eq. (19)], which satisfies the first equation in (18) under the assumption $\kappa D \gg 1$. Thus TBICs are defined predominantly by individual mirrors and in the limit $\kappa D \gg 1$ demonstrate no dependence on the distance between the mirrors $D$. In accordance with the results of Ref. [29], one can show that the TBIC wavefunction amplitude in the propagating mode of the waveguide between the mirrors (25) vanishes under the conditions (26), or (27).

The above discussion of FP BICs and TBICs is rather straightforward and similar to the $\delta$-functional model in Ref. [29] only in the limit $\kappa D \to \infty$. In general, finite $D$ provides inter-mirror interaction through the evanescent waves resulting in nonzero RHS of the first equation in (18). Consequently, conditions (26) or (27), which provide $P = 0$ [see Eq. (19)], are inconsistent with this equation. Thus $B$ in the second equation in (18) is always nonzero. However, in fact, this does not ruin the formation of TBICs, but just renormalizes their energy and parameters by quantities proportional to $e^{-\kappa D}$. Indeed, it can be shown that the conditions (26) or (27) provide both numerator and denominator of the inverse tangent function argument in Eq. (23) to vanish. Thus, in a small vicinity (proportional to $e^{-\kappa D}$) of the energy $E$ and mirror length $L$ near their values $E_{\text{BIC},1}$ and $L_{\text{BIC},1}$ corresponding to a BIC in isolated mirrors [satisfying (26) or (27)], phase $\varphi$ runs through almost all its possible values. Figure 2(a) illustrates the dependence of this phase on energy near BIC in individual mirror. Parameters are chosen as follows: $U = 10$, $V_1 = -2$, $V_2 = 5$, which provide BIC in a single mirror of the lowest possible length to be at $E_{\text{BIC},1} \approx 5.7474$ and $L_{\text{BIC},1} \approx 2.7155$. Hence, the fulfillment of the second equation in the system (18) is achieved for almost any value of $D$ in the vicinity of $E_{\text{BIC},1}$ and $L_{\text{BIC},1}$. Condition $b_1^{s,a} = 0$ derived for TBICs in the case $B = 0$, is violated for finite $D$, in general, but the wavefunction amplitude in the propagating mode between the mirrors remains small: $b_1^{s,a} \sim e^{-\kappa D}$.

Figures 2(b) and 2(c) depict the numerically calculated illustrative examples of the dependence of the BIC energy $E_{\text{BIC}}$ and resonator length $L_{\text{BIC}}$ on the distance between the resonators. Values of the parameters are the same as in Fig. 2(a) with $\theta = 1.1$. Series of periodic in $D$ solutions for $E_{\text{BIC}}$ and $L_{\text{BIC}}$ correspond to FP BICs with the different number of nodes of the wave function between the resonators. The solutions at $E \approx E_{\text{BIC},1}$ and $L \approx L_{\text{BIC},1}$ are almost independent on $D$ and related to the symmetric and antisymmetric TBICs.

Due to the finite length of the mirrors (in contrast to $\delta$-functional model proposed in Ref. [29]), there is a hybridization of TBICs and FP BICs, which takes place near the point of their seeming degeneracy corresponding to the simultaneous fulfillment of $B = 0$ and $\sin(kD/2 + \varphi_{s,a}) = 0$. This hybridization arises because of the coupling between the mirrors through the evanescent modes, and hence it vanishes as $e^{-\kappa D}$ for large distances $D$. It can be shown that there are continuous transitions between FP BIC and TBIC near each point of their apparent degeneracy. Depending on the
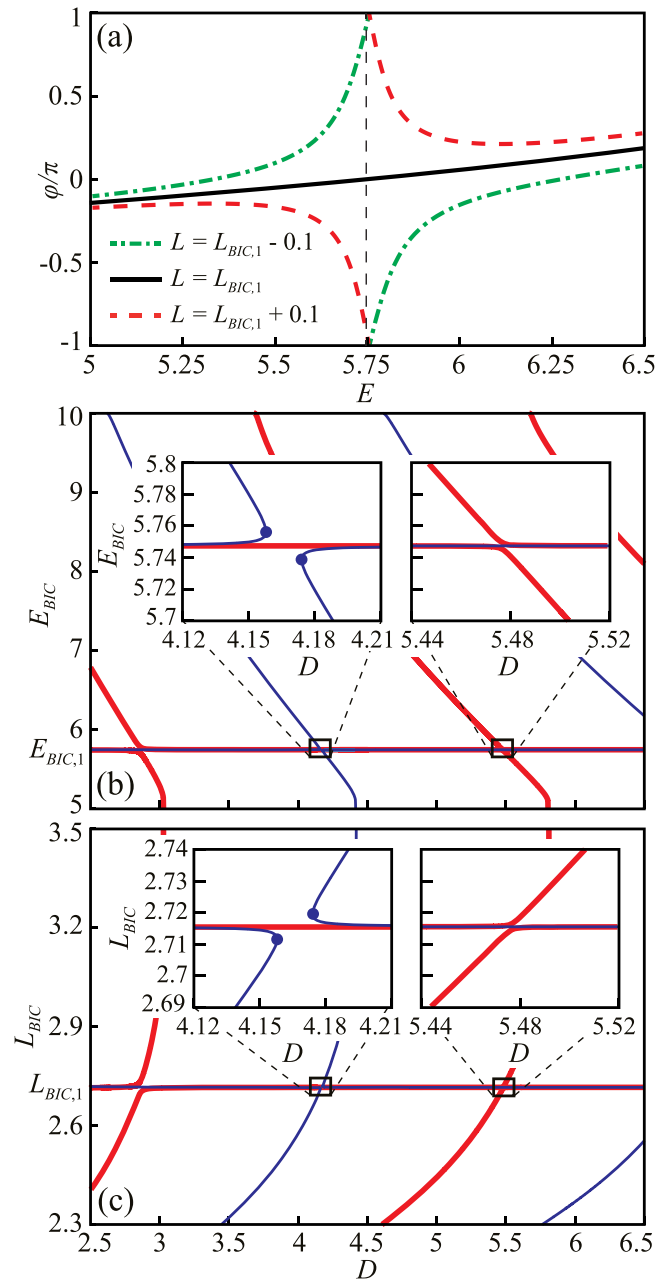
FIG. 2. The phase $\varphi$ of a single mirror reflection amplitude vs energy $E$ (a) for different values of the mirror length $L$ near BIC in the individual mirror at $E_{BIC,1} \approx 5.7474$ and $L_{BIC,1} \approx 2.7155$ (other parameters are specified in the text). The vertical thin dashed black line indicates $E_{BIC,1}$. (b) Dependence of BIC energy $E_{BIC}$ and (c) corresponding resonators length $L_{BIC}$ on a given distance $D$ between the resonators. The red thick and the blue thin lines describe symmetric and antisymmetric BICs respectively. TBICs correspond to the part of these lines, which are almost independent of $D$ and related to the BIC in single resonator at $E \approx E_{BIC,1}$ and $L \approx L_{BIC,1}$. Parts of the lines, which are periodic in $D$, describe FP BICs. The interactions between FP BICs and TBICs are shown in the insets in more details. Merging of antisymmetric BICs with varying $D$ are indicated by dots.

particular system's parameters this transition can provide either repulsion (avoided crossing) or merging of BICs [see insets in Figs. 2(b) and 2(c)].

## III. MERGING AND REPULSION OF FABRY-PÉROT BOUND STATES IN THE CONTINUUM

Recently, merging of BICs in FP resonator was also studied numerically and experimentally in acoustic waveguide [37]. The authors described the mechanism of this merging in a two-level coupled-mode model and suggested a topological origin for BIC merging. Below we show that similar BIC merging phenomenon can be explained by the complicated behavior of Fano antiresonances in the transmission spectrum of individual mirrors. Moreover, resulting BIC merging can be continuously turned into BIC repulsion by an infinitesimal parameter change (as was, in general, proposed in Ref. [48]) making topological nature of this phenomenon questionable.

### A. Merging of Fabry-Pérot bound states in the continuum due to antiresonance coalescence in individual mirrors

The first equation in the system (18) shows that FP BICs are closely related to the Fano resonances (transmission antiresonances) of the single mirror. Recently it was shown in Ref. [35] that antiresonances in a resonator (playing the role of mirror in the FP structure) within a 2D waveguide can demonstrate complicated behavior. In particular, two distinct zero transmission antiresonances can coalesce into one dip with nonzero transmission under variation of the resonator length $L$. Correspondingly, at the same point in the parameter space, one may expect merging of two FP BICs in the FP configuration, which are associated with those two transmission zeros of individual mirrors.

Figure 3 depicts an example of the dependence of BICs energy and corresponding FP cavity length on the length of the individual mirror in the vicinity of a point of antiresonance coalescence. Parameters of the structure are the following: $U = 10$, $V_1 = -2$, $V_2 = 5$, and $\theta = 1.1$. Analyzing function $P(E)$ from Eq. (19) for these parameters, one can derive that there are several possible transmission zero coalescence regimes in a single mirror for the particular parameters chosen. Antiresonance coalescence for the smallest length $L$ takes place at $E_0 \approx 5.7522$ and $L_0 \approx 1.4754$ (shown by straight thin dashed black lines in Fig. 3). In the vicinity of $L_0$, there are two distinct perfect reflection antiresonances of the single mirror for $L < L_0$ and no perfect reflection of the single mirror in this energy range for $L > L_0$ [35]. Thus it is expected, that there will be two distinct BICs for $L < L_0$ related to two distinct transmission antiresonances of the mirror and no BICs for $L > L_0$. Indeed, one can see from Fig. 3, that there is a pair of BICs with energies close to $E_0$ for $L \lesssim L_0$, which merge at $E \approx E_0$ and $L \approx L_0$, and no BICs remain present in this energy range for $L \gtrsim L_0$. Inset in Fig. 3(a) demonstrates the change of $Q$-factor (inverse imaginary part $\Gamma$ of the $S$-matrix pole) behavior during BIC merging with variation of $L$.

Merging of symmetric BICs takes place for mirror length slightly shorter than $L_0$, whereas antisymmetric BICs merge for mirror length slightly longer than $L_0$. The reason for this is the coupling between the mirrors through the evanescent mode of the FP cavity, which provides nonzero RHS of opposite sign for symmetric and antisymmetric cases in the first equation in Eqs. (18). This coupling decays exponentially as the distance between the mirrors increases. Hence, the
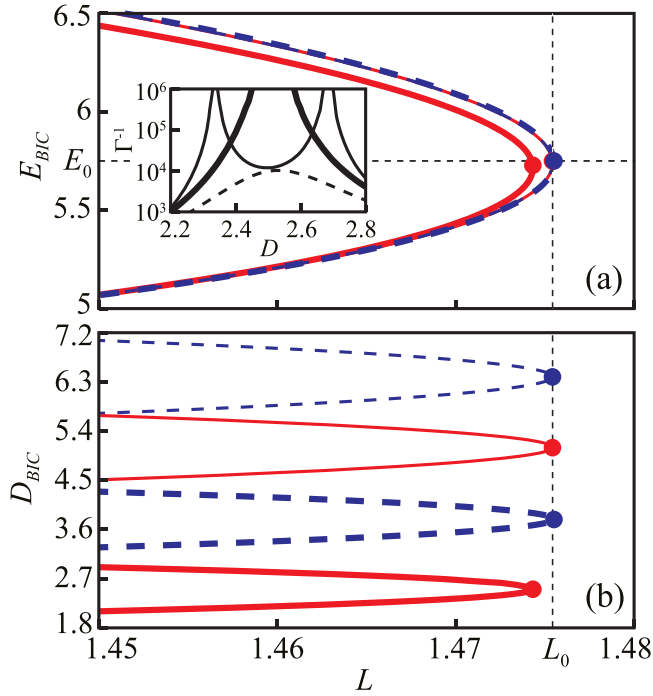
FIG. 3. Dependence of BIC energy $E_{BIC}$ (a) and corresponding distance between the resonators $D_{BIC}$ (b) on a given resonator length $L$. The red solid thick and thin lines are related to the symmetric BICs, and the blue dashed thick and thin lines—to the antisymmetric BICs. Parameters are specified in the text. Merging of BICs (shown by red and blue dots) takes place near the coalescence of antiresonances in a single resonator at $E_0 \approx 5.7522$ and $L_0 \approx 1.4754$ (indicated by thin dashed black lines). Inset in part (a): $Q$-factor (inverse imaginary part $\Gamma$ of the $S$-matrix pole) vs distance between the resonators for $L = 1.47$ (thin solid line), $L \approx 1.4743$ (thick solid line), and $L = 1.48$ (thin dashed line).

merging point of FP BICs becomes closer and closer to the point of antiresonance coalescence ($L = L_0$ and $E = E_0$) with increasing number $n$ of the FP resonances involved in the BIC formation [increasing $D$ in accordance with Eq. (3)]. Moreover, Fig. 3(b) shows that this phenomenon is (almost) periodic in $D$ as it is expected for BICs of Fabry-Pérot type.

Coalescence of antiresonances is a common phenomenon in transmission properties of structures possessing several tunneling paths [19,38,49], and, in contrast to the model of BIC merging proposed in Ref. [37], it does not obligatory require evanescent mode coupling to take place. Therefore merging of BICs arising from the coalescence of antiresonances can be studied in a tight-binding toy-model as well (see Appendix B for details) that demonstrates the versatility of the effect.

### B. Continuous transition between merging and repulsion of bound states in the continuum

Behavior of antiresonances in the transmission spectrum of an individual mirror is rather complicated, in general, and the aforementioned coalescence of antiresonances can be transformed into crossing and avoided crossing of antiresonances [35,38]. This transition is provided by a continuous change of a certain parameter. In the considered case of a resonator in a waveguide, one can tune the coupling matrix elements (8)

to observe such a transition [35]. Figures 4(a)–4(c) depict an example of the transmission coefficient spectrum dependence on the resonator length of a single mirror within the two-mode approximation for different values of parameter $\theta$, which governs coupling matrix elements in accordance to Eq. (9).

In the FP configuration, we expect that such behavior of transmission antiresonances of individual mirrors manifests itself in the corresponding behavior of FP BICs. Figure 4(d) shows the dependence of the distance between the mirrors required for the formation of the first four pairs (counting from $D = 0$) of symmetric and antisymmetric FP BICs on the length of the individual mirror. Behavior of energy of these BICs is illustrated in Figs. 4(e)–4(h). Variation of the parameter $\theta$ in each mirror transforms their individual antiresonances. However, FP BICs do not follow individual resonators transmission dips exactly due to evanescent modes coupling between the mirrors resulting in the nonzero RHS of the first equation in system (18).

For large $D$, factor $e^{-\kappa D}$ becomes negligible and BICs do repeat the behavior of antiresonances and, in particular, demonstrate the transition from merging, which correspond to the coalescence of antiresonances at $\theta = 0.73$, to their repulsion (avoided crossing) at $\theta = 0.72$ [see the second pairs of symmetric and antisymmetric BICs in Fig. 4(d) and Figs. 4(g) and 4(h), respectively]. Nevertheless, the very crossing regime for BICs is slightly shifted in the respect to the crossing of antiresonances because of still nonzero coupling between the mirrors. On the other hand, for smaller $D$, RHS of the first equation in system (18) is sufficient to prevent the change of BIC behavior under a small variation of parameters near the coalescence-avoided-crossing transition of the individual mirror antiresonances. For instance, the first symmetric FP BICs merge at $\theta = 0.72$ and 0.73, whereas the first antisymmetric BICs demonstrate repulsion for both $\theta = 0.72$ and 0.73 [see the first pairs of symmetric and antisymmetric BICs in Fig. 4(d) and Figs. 4(e) and 4(f), respectively].

Previously, it was proposed in the literature that there is a strong dependence of the $Q$-factor on the parameters detuning from their values corresponding to the very point of BIC merging [36,37]. However, as we show here, this is not a specific property of the BIC merging point. Such a behavior of the $Q$-factor is defined primarily by the path in the parameters space, along which the evolution of $Q$-factor is studied, rather than by the particular chosen point on the BIC existence curve. For instance, let us consider the repulsion (not merging!) of the symmetric FP BICs near $L \approx 1.8$ and $D \approx 3$ [see Figs. 4(d) and 4(g)] for $\theta = 0.72$. Figure 5(a) shows the BIC existence curve in the $D$-$L$ parameter space and two different paths in this space, along which one can study the $Q$-factor (inverse imaginary part $\Gamma$ of the $S$-matrix pole) asymptotic in the vicinity of BIC at $L = L_{BIC} = L_t = 1.78$ and $D = D_{BIC} \approx 3.17443$. Dependence of the $Q$-factor on the detuning $\Delta L = L - L_t$ along the line tangent to the BIC existence curve is $Q \sim \Gamma^{-1} \sim \Delta L^{-4}$, which is stronger than along any other intersecting line $Q \sim \Delta L^{-2}$ [Fig. 5(b)]. This is due to the properties of the path in the parameter space, not the specific BIC point considered (see Appendix C). In the case of BIC merging point, tangent line is parallel to one of the parameters axis, just providing a simpler analysis of this effect. Thus, in fact, merging and repulsion of BICs in finite
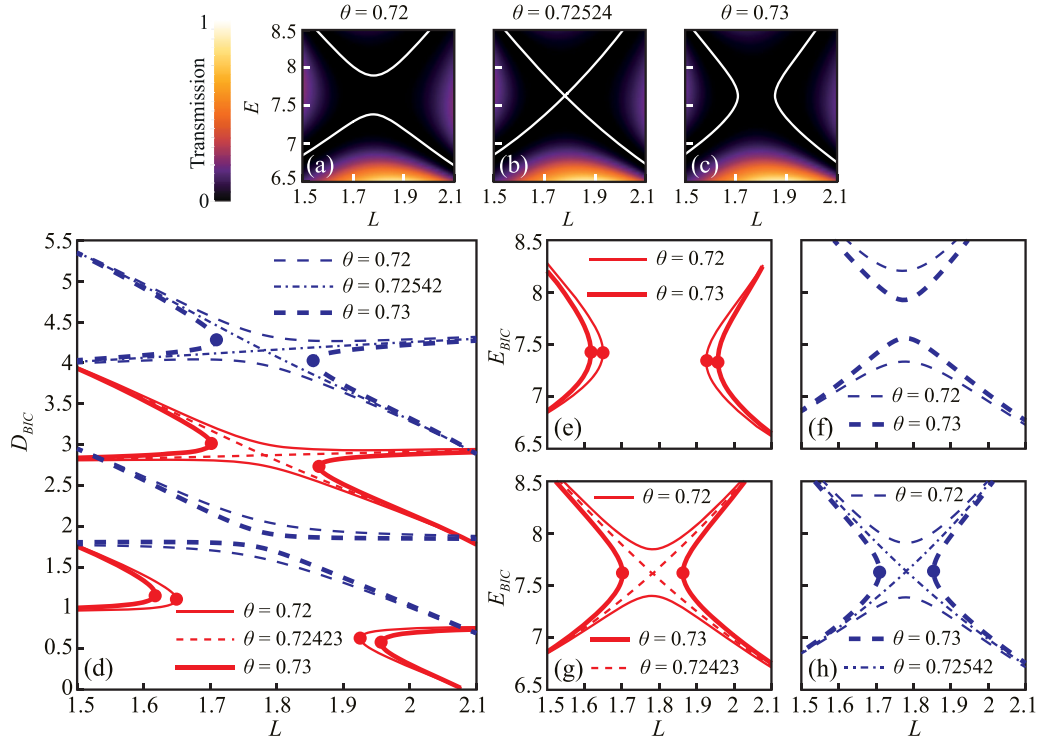
FIG. 4. Energy-vs-resonator-length diagrams of the single mirror transmission coefficient for $\theta = 0.72$ (a), $\theta \approx 0.72524$ (b), and $\theta = 0.73$ (c), which correspond to antiresonance repulsion (avoided crossing), crossing and coalescence respectively. Zero transmission antiresonances are shown by white lines. The rest parameters are as follows: $U = 10$, $V_1 = -2$, $V_2 = 5$. (d) Distance between the mirrors $D_{\text{BIC}}$ corresponding to a few first FP BICs (red lines are denoted to symmetric and blue lines—to antisymmetric states) and [(e)–(h)] respective BICs energy vs given length $L$ for different values of $\theta$: symmetric FP BICs near $D_{\text{BIC}} \approx 1$ (e), $D_{\text{BIC}} \approx 3$ (g) and antisymmetric FP BICs near $D_{\text{BIC}} \approx 2$ (f), $D_{\text{BIC}} \approx 4$ (h).

systems are closely related to each other and differ just by a corresponding rotation of the parametric space.

Nevertheless, we should admit that BIC merging point in systems with guided modes is indeed specific in the context of $Q$-factor asymptotic behavior. In such systems, in the case of BIC merging, $Q$-factor blows up as $\Delta k^{-4}$ along any direction in the specified momentum space [23,26,30,31]. It can be



FIG. 5. (a) Dependence of the distance between the resonators, required for a symmetric BIC formation, on a given resonator length $L$ (thick red line). Thin solid and dashed black lines correspond to tangent and intersecting lines to the BIC existence curve $D = D_{\text{BIC}}(L)$ at the point $L = L_t = 1.78$ and $D = D_{\text{BIC}}(L_t) \approx 3.17443$. (b) Dependence of the $Q$-factor (inverse imaginary part $\Gamma$ of the $S$-matrix pole) on the detuning $\Delta L = L - L_t$ along the paths shown in part (a).

described in the following way. A hyperplane "tangent" to the BIC existence manifold in the combined space of parameters and momentum becomes parallel to the momentum subspace. Thus any detuning in the momentum is a tangent to the BIC existence hypersurface resulting in corresponding strong behavior of the $Q$-factor.

## IV. NUMERICAL CALCULATIONS

### A. Two-dimensional quantum-mechanical waveguide with two expansions

As a quantum-mechanical model structure for numerical simulations we consider a 2D waveguide of width $h$ with two identical expansions of width $H > h$ playing role of mirrors [inset in Fig. 6(a)]. A FP resonator cavity is represented by a waveguide of width $h_0$ between the expansions. Potential energy inside the waveguide and resonators is set as the energy origin and outside the waveguide [gray shaded region in the inset in Fig. 6(a)] it is $U_0 = 1$ eV. To be specific, the effective mass of the electron is chosen to be $0.0665m_0$ (typical value in GaAs-based materials). We solve the scattering problem for the Schröedinger equation (4) and identify BICs as Fano resonances with a vanishing split between a peak and a dip [19,34].

The full numerical solution of the 2D Schröedinger equation by the transverse modes decomposition requires infinitely many eigenstates of Eq. (5) belonging to both discrete and continuous spectra to be considered. The transverse modes of
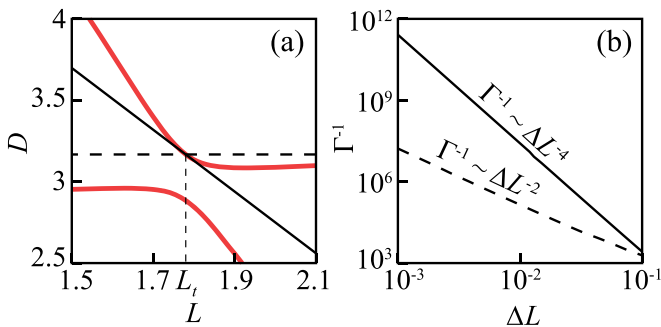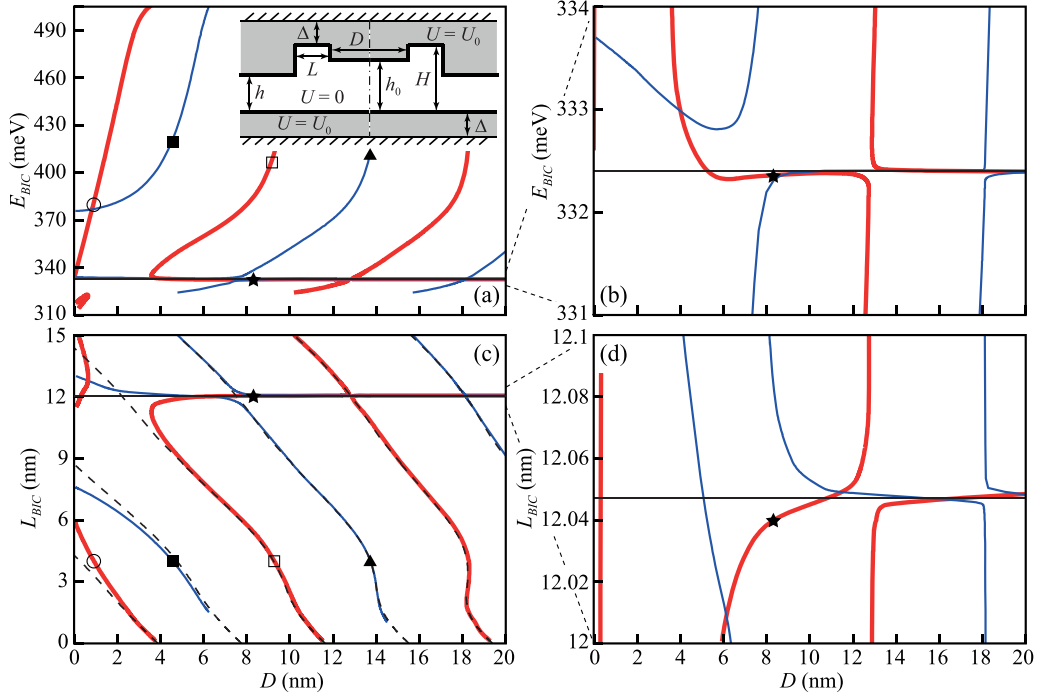
FIG. 6. [(a) and (b)] Numerically calculated dependence of BIC energy $E_{BIC}$ and [(c) and (d)] corresponding resonators length $L_{BIC}$ on a given distance $D$ between the resonators. The red thick and the blue thin lines describe symmetric and antisymmetric BICs respectively. The symmetric waveguide structure under study is shown in the inset in part (a), parameters are specified in the text. The black thin solid line indicates the energy $E_{BIC,1} \approx 332.398$ meV and the corresponding resonator length $L_{BIC,1} \approx 12.047$ nm of the BIC in the isolated resonator. Away from the BIC of individual resonator, BIC in the whole structure follows the effectively single-mode FP phase matching condition (3) [see thin black dashed lines in part (c)]. Points indicate BICs illustrated by probability density distribution in Fig. 7.

the continuous spectrum are simulated numerically by a dense set of discrete modes formed between artificial infinite potential borders located at some distance $\Delta$ from the structure [inset in Fig. 6(a)]. The true continuous spectrum corresponds to $\Delta \to \infty$ and the number $N$ of transverse modes taken into account being infinite. For the particular parameters, we tune $\Delta$ and $N$ consistently until simulation results begin to demonstrate weak dependence on them. In the present paper, it took place for $\Delta \gtrsim 2.5$ nm and $N \geqslant 10$, thus, for convenience of numerical calculations, we set $\Delta = 2.5$ nm and $N = 10$.

### 1. Fabry-Pérot and twin bound states in the continuum with locally symmetric mirrors

At first, we consider waveguide between the expansions to have the same width as outside them ($h_0 = h$) providing mirrors to be locally symmetric (surrounded by waveguides of the same width). We begin with the simplest case when coalescence of antiresonances in the individual mirror is absent. For low energy antiresonances, this can be guaranteed either by $|\mu_{21}| \gg |\mu_{22}|$ ($\theta \ll 1$ within two-mode approximation) or $|\mu_{21}| \ll |\mu_{22}|$ ($|\pi/2 - \theta| \ll 1$ within two-mode approximation). The former can hardly be achieved in a realistic structure, so we focus on the case $|\mu_{21}| \ll |\mu_{22}|$, which requires that $h$ and $H$ do not differ much [34,35]. Specifically, we take $h = 5$ nm and $H = 7$ nm that provides $\mu_{22} \approx 0.753$ and $\mu_{21} \approx -0.260$. The energy range of interest is restricted between the thresholds of the second transverse mode in mir-

rors $\xi_2^{2,4} \approx 306.3$ meV and the second transverse mode in waveguide $\xi_2^{1,3,5} \approx 507.7$ meV.

Figure 6 depicts numerically calculated BICs existence curves in the $E$-$L$ and $D$-$L$ coordinate planes. Similar to the analytical two-mode model, two types of BICs can be clearly distinguished for large $D$: periodic in $D$ FP BICs and TBICs related to the BIC in isolated mirrors at $L_{BIC,1} \approx 12.047$ nm and $E_{BIC,1} \approx 332.398$ meV, which are almost independent on $D$. We admit that precise numerical calculation approves that FP BICs indeed accurately follow the phase matching condition (3) [see Fig. 6(c)]. The key difference between FP BICs and TBICs can be highlighted by their wave functions (Fig. 7). As expected from the two-model analytical consideration, FP BICs have nonzero probability distribution between the resonators, whereas TBICs are localized almost within mirrors with vanishingly small wavefunction amplitude between them. If the parameters of the FP BIC bring it close to the TBIC, they interfere, and the continuous transition between them is observed, as was predicted within the two-mode model [compare Fig. 2 and Figs. 6(b) and 6(d)]. For small $D$, FP BICs and TBICs become strongly hybridized due to large evanescent mode coupling between the mirrors. One can check that in the limit $D \to 0$ numerically calculated BICs also tend to the BICs in a single resonator (mirror) of double length $2L$. These results are similar to the Ref. [29], where the FP resonator was considered with mirrors formed by scattering regions with attractive potential ("impurities" or quantum wells [42]) inside a uniform waveguide. Thus we
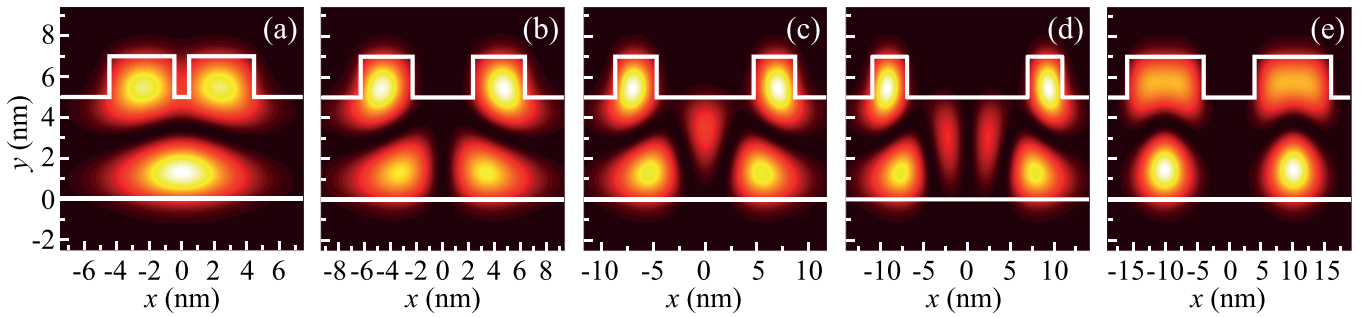
FIG. 7. [(a) and (c)] Probability density distribution in the symmetric and [(b) and (d)] antisymmetric FP BICs and in the symmetric TBIC (e). FP BICs correspond to $L_{BIC} = 4$ nm, $E_{BIC} \approx 379.720$ meV and $D_{BIC} \approx 0.897$ nm [open circle in Fig. 6(a)], $E_{BIC} \approx 418.303$ meV and $D_{BIC} \approx 4.631$ nm [filled square in Fig. 6(b)], $E_{BIC} \approx 411.011$ meV and $D_{BIC} \approx 9.316$ nm [open square in Fig. 6(c)], and $E_{BIC} \approx 411.884$ meV and $D_{BIC} \approx 13.78$ nm [filled triangle in Fig. 6(d)]. TBIC corresponds to $L_{BIC} \approx 12.04$ nm, $D_{BIC} \approx 8.02$ nm, and $E_{BIC} \approx 332.355$ meV [filled star in Fig. 6(e)].

have explicitly demonstrated that the formation of TBICs is not a model-specific but a universal phenomenon.

### 2. Merging of Fabry-Pérot bound states in the continuum due to antiresonance coalescence

As we have shown above, within the two-mode model, coalescence of antiresonances in individual resonators (mirrors of the FP resonator) manifests in merging of FP BICs. Coalescence of antiresonances in the transmission spectrum of a single resonator in 2D waveguide, typically, takes place for $|\mu_{22}| \ll |\mu_{12}|, |\mu_{21}|$ [35]. Naturally, this can be provided under the condition $h \sim H/2$, so we choose $h = 10$ nm and vary $H$ in the vicinity of $H \sim 20$ nm.

Figure 8(a) depicts the dependence of a single mirror (shown in the inset) transmission spectrum on its length $L$. There are two regions in the $E$-$L$ space shown in Fig. 8(a), where we study coalescence of antiresonances. Coalescence in the region $A$ is almost independent of the matrix element $\mu_{22}$ and takes place for a wide range of $H$ values, because it lies above the threshold of the third mode in resonators and it is formed due to multimode interference. On the other hand, coalescence of antiresonances in the region $B$ is of the two-mode interference nature and is very sensitive to the value of $\mu_{22}$ matrix element (consequently, to the value of $H$). For the particular values of the parameters, crossing of antiresonances, i.e. the very transition regime between avoided crossing and coalescence, corresponds to $H_0 \approx 21.737$ nm [Figs. 8(b)–8(d)].

Merging of FP BICs related to the antiresonance coalescence in a single resonator in region $A$ [see Fig. 8(a)] is illustrated by Fig. 9, where the dependence of the BIC energy $E_{BIC}$ and the corresponding distance between the mirrors $D_{BIC}$ on the length $L$ is presented. As expected, BIC merging takes place almost at the same energy and mirror length that corresponds to antiresonance coalescence (shown by thin black dashed lines). Similar to the predictions of the two-mode model (Fig. 3), merging of FP BICs provided by coalescence of antiresonances is almost periodic in $D$.

As we have noticed above, within the two-mode model, a continuous transformation of the antiresonance behavior from avoided crossing to crossing and then – to coalescence provides similar behavior of FP BICs (see Fig. 4). Similar

phenomenon is confirmed within the full numerical simulation. Figure 10(a) shows the dependence of FP cavity length $D$ corresponding to BICs in the region $B$ of the $E$-$L$ space of an isolated resonator [Fig. 8(a)]. Parameters are chosen
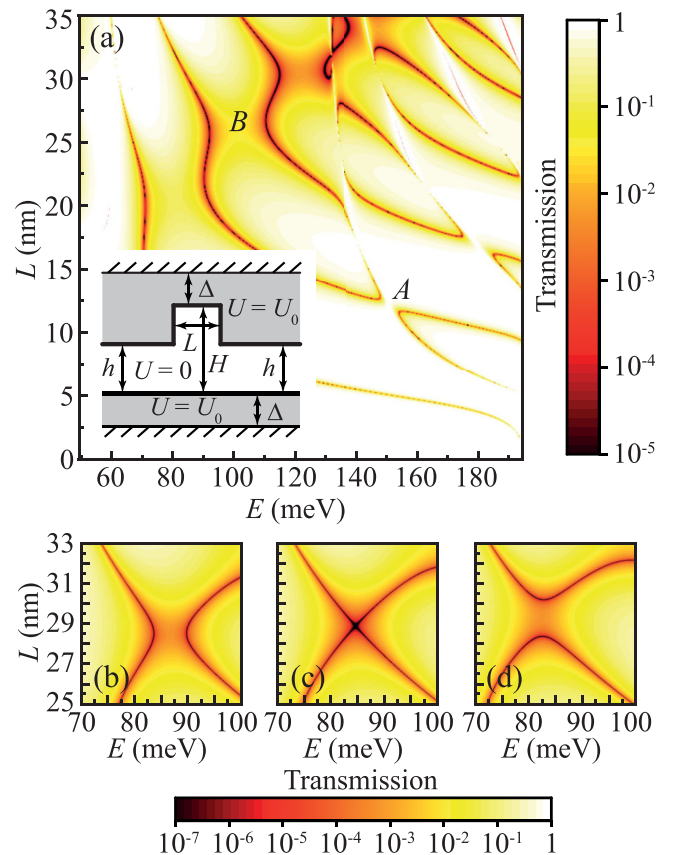


FIG. 8. Numerically calculated energy-vs-resonator-length diagrams of the single mirror transmission coefficient for $h = 10$ nm and $H = 20$ nm (a). The structure of the considered single mirror is shown in the inset. Regions, where antiresonance coalescence is studied are labeled by $A$ and $B$. Evolution of the transmission coefficient spectrum in the region $B$ from the avoided crossing of antiresonances at $H = 21.5$ nm (b) to crossing at $H = H_0 \approx 21.737$ nm (c), and coalescence of antiresonances at $H = 22$ nm (d).
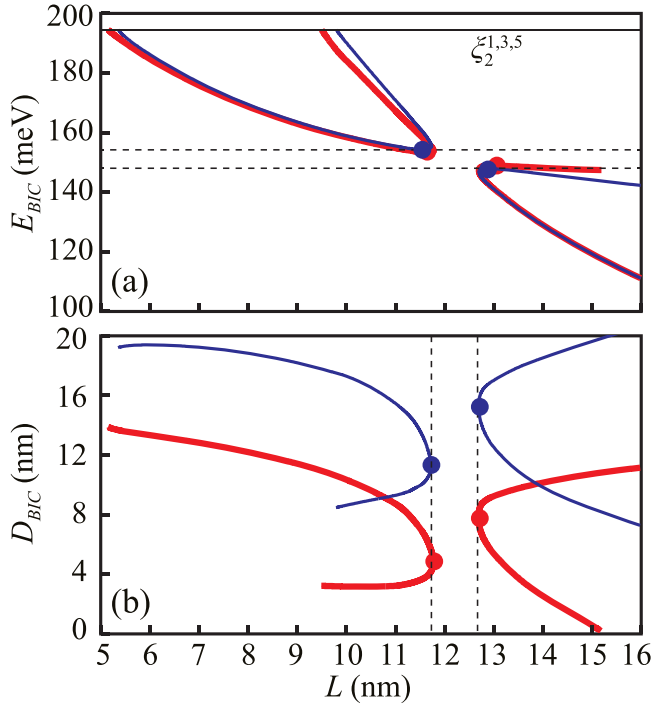
FIG. 9. Numerically calculated dependence of BIC energy $E_{BIC}$ (a) and corresponding distance between the mirrors $D_{BIC}$ (b) on a given mirror length $L$ in the region $A$ [see Fig. 8(a)]. The red thick lines are related to the symmetric BICs, and the blue thin lines – to the antisymmetric BICs. Parameters are the following: $h = 10$ nm and $H = 20$ nm. $\xi_2^{1,3,5} \approx 194.5$ meV is the threshold of the second transverse mode in the waveguides. Merging of BICs (shown by red and blue dots) takes place near the coalescence of antiresonances at $E_0 \approx 148.0$ meV and $L_0 \approx 12.68$ nm or $E_0 \approx 154.2$ meV and $L_0 \approx 11.74$ nm (indicated by thin dashed black lines).

to be detuned from the exact antiresonance crossing condition $H = H_0 \approx 21.737$ nm [Fig. 8(c)] either towards the avoided crossing of antiresonances ($H = 21.5$ nm) or to the coalescence of antiresonances ($H = 22$ nm). Qualitative difference in the BIC behavior can be illustrated by studying the $Q$-factor (inverse imaginary part $\Gamma$ of the $S$-matrix pole). Figures 10(b) and 10(c) show the dependence of the $Q$-factor on $D$ for different values of $L$ and $H$ near the antisymmetric FP BICs. In the case of BIC merging ($H = 22$ nm), $Q$-factor has either two, one, or no divergent points in agreement with the analytical model [see inset in Fig. 3(a)]. On the other hand, in the case of BIC repulsion ($H = 21.5$ nm), there are always two divergent points in the parameters range of interest. We also admit, that transition between BIC merging and repulsion takes place under infinitesimal parameter change. Figure 10(d) depicts the dependence of $D$ corresponding to FP BICs for $H_0 > H = 22.73$ nm and $H_0 < H = 22.74$ nm. Transition from merging to repulsion is observed only for antisymmetric BICs for larger $D$ (see the behavior of antisymmetric BICs near $D_{BIC} \sim 16$ nm in Fig. 10), while symmetric BICs for smaller $D$ demonstrate the same behavior (merging) for both values of $H$ (symmetric BICs in the case shown in Fig. 10 at $D \sim 4$ nm). The reason for this is that coupling between the mirrors through the evanescent modes becomes negligible for large $D$.
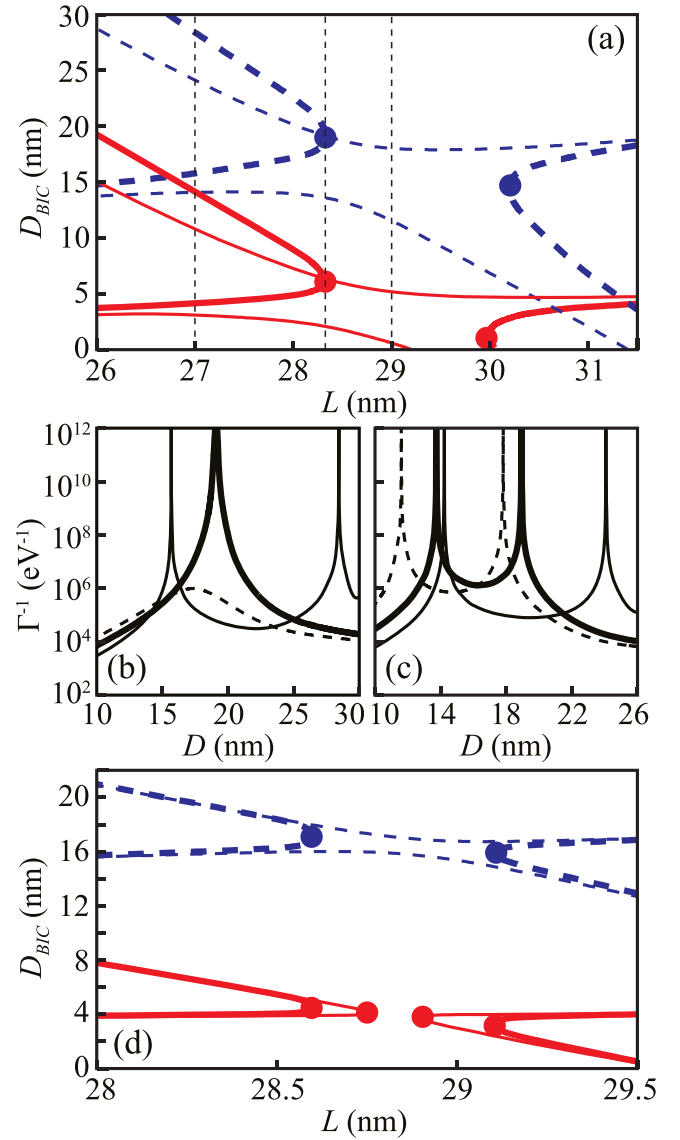


FIG. 10. Numerically calculated dependence of the distance between the mirrors corresponding to BIC $D_{BIC}$ (a) on a given length $L$ in the region $B$ [see Fig. 8(a)]. The red solid lines are related to the symmetric BICs, and the blue dashed lines to the antisymmetric BICs. Parameters are the following: $h = 10$ nm and $H = 21.5$ nm (thin lines) or $H = 22$ nm (thick lines). $Q$-factor (inverse imaginary part $\Gamma$ of the $S$-matrix pole) of the first pair of antisymmetric BICs vs. distance between the resonators for $H = 22$ (b) and 21.5 nm (c). Thin solid line corresponds to $L = 27$ nm, thick solid line – to $L = 28.35$ nm, and thin dashed line to $L = 29$ nm [labeled by vertical thin dashed lines in part (a)]. Numerically calculated dependence of the distance between the mirrors corresponding to BIC $D_{BIC}$ (d) on a given length $L$ for $H = 21.73$ nm (thin lines) and $H = 21.74$ nm (thick lines).

### 3. Twin bound states in the continuum in resonator with locally asymmetric mirrors

Let us allow the interior waveguide of the FP cavity to have width different to the exterior waveguide width ($h_0 \neq h$). Thus waveguide expansions playing the role of mirrors will become locally asymmetric (waveguides to the left and to the right from the each mirror are different). De-
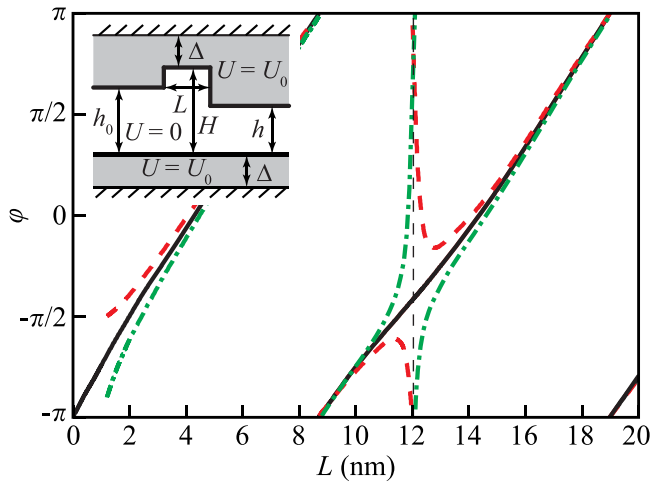
FIG. 11. Phase of the reflection amplitude of the individual mirror (shown in the inset) at the energy of its full opaqueness. Black solid line corresponds to $h_0 = h = 5$ nm, red dashed line – to $h > h_0 = 4.8$ nm and green dot-dashed line to $h < h_0 = 5.2$ nm. Thin dashed vertical line indicates the length $L_{BIC,1} \approx 12.047$ nm, corresponding to BIC in an isolated symmetric ($h_0 = h = 5$ nm) mirror.

structive interference providing Fano antiresonances in the transmission spectrum of individual mirror remains in the asymmetric case. However, FW mechanism of BIC formation in asymmetric expansion does not work unless additional condition of proportionate coupling (A3), (A4) is fulfilled [34]. Nevertheless, as we show below, this condition is not obligatory to observe BICs weakly depending of $D$ (TBICs) in the vicinity of energy $E$ and parameter $L$ near their values $E_{BIC,1}$ and $L_{BIC,1}$ corresponding to BIC in individual locally symmetric mirror.

The phase $\varphi$ of the reflection amplitude of an individual locally asymmetric mirror also demonstrates sharp behavior near the BIC point in the energy-parameter space, which is similar to the case of locally symmetric mirrors illustrated in Fig. 2(a). Figure 11 shows the numerically calculated phase $\varphi$ of the individual mirror (expansion of width $H = 7$ nm in a waveguide of width $h = 5$ nm – see inset in Fig. 11) under the condition of perfect opaqueness (Fano antiresonance) as a function of its length. In the symmetric case, where BIC in the isolated mirror can be formed, phase is smooth and continuous. As soon as the mirror becomes asymmetric, there is a sharp $\pm 2\pi$ change of the phase near the mirror length $L_{BIC,1} \approx 12.047$ nm, corresponding to BIC in symmetric case. Moreover, one can see that this change is of different sign for $h > h_0$ and $h < h_0$. In particular, the dependence $\varphi(L)$ is monotonic for $h < h_0$ and nonmonotonic for $h > h_0$.

Such a sharp dependence of the reflection amplitude phase naturally provides features of the BIC behavior in the FP configuration similar to TBICs in the case of symmetric mirrors. Indeed, according to Fig. 12, where BIC existence curves in FP structures with asymmetric mirrors are shown, in both cases ($h > h_0$ and $h < h_0$) either symmetric and antisymmetric BICs demonstrate a weak dependence on $D$ for mirror length in the vicinity of $L_{BIC,1} \approx 12.047$ nm, corresponding to BIC in an isolated symmetric ($h_0 = h = 5$ nm) expansion. In accordance with the behavior of the reflection amplitude
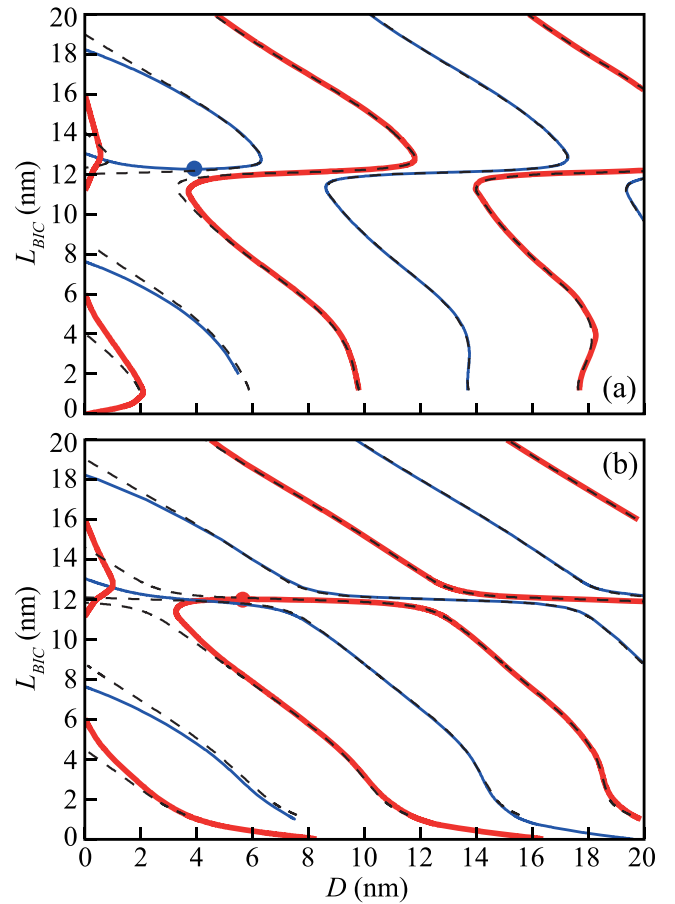


FIG. 12. Numerically calculated dependence of individual mirrors lengths $L_{BIC}$ corresponding to BIC formation on a given distance $D$ between them. The red thick and the blue thin lines describe symmetric and antisymmetric BICs respectively. The width $h_0$ of the central waveguide is $h > h_0 = 4.8$ nm (a) and $h < h_0 = 5.2$ nm (b). Black dashed lines show the effectively single-mode FP phase matching condition (3). Merging of symmetric and antisymmetric BICs are labeled by red and blue dots, respectively.

phase (Fig. 11), dependence $D(L_{BIC})$ is monotonic for $h < h_0$ and nonmonotonic for $h > h_0$. The main difference between structures with $h_0 \neq h$ and with locally symmetric mirrors ($h_0 = h$) is the following. In the former case, there is a continuous transition between FP resonances with increase (for $h > h_0$) or decrease (for $h < h_0$) of its FP resonance number $n$ by 2 for both symmetric and antisymmetric BICs with increase of $L$ through the value $L_{BIC,1}$. Whereas in the case of symmetric mirrors, there is increase of $n$ for symmetric and decrease of $n$ for antisymmetric BICs (compare Fig. 12 with Fig. 6).

One can see that in Fig. 12 there is also a good agreement between the precise numerical simulations and the approximate single-mode calculations through the FP phase matching condition (3). Differences take place at small $D$, where evanescent coupling between the mirrors is not negligible. These differences are mainly quantitative, but there are two main qualitative features. First, the existence of the symmetric BIC with the lowest $L$ in the limit $L \to 0$ and $D \to 0$ for $h > h_0$, which is absent within the single-mode

phase analysis [Fig. 12(a)]. This BIC is the only one, which survives in the system with $h > h_0$ in the limit $L \rightarrow 0$. Second, merging of antisymmetric (symmetric) BICs with decrease (increase) of the single mirror length for $h > h_0$ ($h < h_0$). Mechanism of this merging is different to the proposed above coalescence of antiresoannces in single mirror, and, as we have demonstrated, it is of multimode nature. We also admit that, in contrast to the case $h > h_0$, structures with $h < h_0$ possess BICs in the limit $L \rightarrow 0$ and $D \neq 0$, which tend to corresponding BICs in a single resonator of length $D$ and width $h_0 > h$ [see Fig. 12(b)]. The antisymmetric BIC with the lowest $L$ and $D$ does not exist in the limit $L \rightarrow 0$ in the particular example considered because corresponding BIC in the single resonator limit is absent as its energy goes above the threshold of the second transverse mode in the external waveguides.

### B. Two-dimensional optical Fabry-Pérot resonator

Due to deep connection between Schröedinger and Helmholtz equations [50], one can expect qualitative agreement between behavior of BICs in quantum-mechanical and optical systems. To be more specific, we consider Helmholtz equation for $z$ component of the electric field $\mathcal{E}_z$ (TE polarization) in the 2D dielectric waveguide with propagation direction along the $x$ axis. In this case, the Helmholtz equation is equivalent to Eq. (4) for $\tilde{\Psi}(x, y) = \mathcal{E}_z(x, y)$ with factor $E - U(x, y)$ being substituted by $q_0^2 \varepsilon(\omega, x, y)$:

$$\frac{\partial^2 \tilde{\Psi}}{\partial x^2} + \frac{\partial^2 \tilde{\Psi}}{\partial y^2} + q_0^2 \varepsilon(\omega, x, y) \tilde{\Psi} = 0, \qquad (28)$$

where $q_0 = \omega/c$ is the wave vector in free space, $\omega$ is the frequency, $c$ is the speed of light, and $\varepsilon(\omega, x, y)$ is the distribution of the dielectric constant over the system.

The main difference between 2D waveguides, whose description is based either on Schröedinger or Helmholtz equations, is that in the latter case there are no bound states and hence no Fano resonances in infinite single-connected optical waveguides. Bound states and Fano resonances appear only after introduction of metal boundaries restricting wave motion in the direction $y$ perpendicular to the propagation direction $(x)$. This can be qualitatively explained in the following way.

In dielectric structures, the sign of the term $q_0^2 \varepsilon(\omega, x, y)$ is fixed and positive contrary to quantum mechanics, where difference $E - U(x, y)$ can acquire both positive and negative values. Moreover, the degree of freedom related to independent variation of energy $E$ and potential $U(x, y)$ is absent in electrodynamics. It is instructive to rewrite the Helmholtz equation following Ref. [10] in the form similar to the Schröedinger equation with effective potential energy $\tilde{U}(x, y) = q_0^2 [1 - \varepsilon(\omega, x, y)]$ instead of $U(x, y)$ in Eqs. (4) and (5), and effective energy $\tilde{E} = q_0^2$ standing for $E$ in Eqs. (4) and (6):

$$q_0^2 \varepsilon(\omega, x, y) = \tilde{E} - \tilde{U}(x, y) = q_0^2 - q_0^2 [1 - \varepsilon(\omega, x, y)]. \quad (29)$$

Hence, in electrodynamics, we have an analog of the Schröedinger equation but with fixed and positive effective energy.

Consider, as we have done it in quantum-mechanical numerical calculations above, a structure with a piecewise constant $\varepsilon$ in the $x$ direction. Thus we can divide the system into regions along propagation direction, where in the $j$th region, we have $\varepsilon(x, y) = \varepsilon_j(y)$. Similarly to the 2D Schröedinger equation (4), we solve this Helmholtz equation by the variable separation. However, to get a qualitative insight, we suppose here that there is a single transverse mode in each region, contrary to an exact numerical simulation. Thus, in the $j$th region, one gets the Helmholtz equation for the transverse function $\tilde{\chi}^j(y)$ of the electric field $\tilde{\Psi}_j(x, y) = \tilde{\psi}^j(x) \tilde{\chi}^j(y)$ similar to Eq. (5):

$$\frac{\partial^2 \tilde{\chi}^j(y)}{\partial y^2} + [\tilde{\xi}^j - \tilde{U}_j(y)] \tilde{\chi}^j(y) = 0. \qquad (30)$$

Here $\tilde{\xi}^j$ is the separation constant, which determines the threshold of a mode propagating in $y$ direction, and $\tilde{U}_j(y) = \omega^2/c^2 [1 - \varepsilon_j(y)]$ is the effective potential in the $j$th region. Inside the waveguide $\varepsilon_j(y) > 1$ ($\tilde{U}_j(y) < 0$) and outside – $\varepsilon_j(y) = 1$ ($\tilde{U}_j(y) = 0$). Therefore, along the $y$ axis perpendicular to the propagation direction, we have a standard 1D quantum well problem. Localized in the $y$ direction solution corresponds to eigenenergy $\tilde{\xi}^j < 0$. Propagation along the $y$ axis is described by $\tilde{\xi}^j > 0$.

Along the $x$ axis in each region, the Helmholtz equation reads similar to Eq. (6) giving the solution $\tilde{\psi}^j(x) = \exp(\pm i \beta^j x)$, where we have introduced a waveguide propagation constant $\beta^j$. From Eq. (6), it immediately follows that

$$(\beta^j)^2 = \tilde{E} - \tilde{\xi}^j = q_0^2 - \tilde{\xi}^j, \qquad (31)$$

which illustrates the well-known fact that the propagation constant of waveguide mode (evanescent outside the waveguide in the $y$ direction with $\tilde{\xi}^j < 0$) should be larger than the free space wave vector.

BICs require spatial localization along both $x$ and $y$ axis. Localization along the $x$ axis formally corresponds to $(\beta^j)^2 < 0$. To study the possibility of such localization, we assume that functions $\tilde{\psi}^j(x)$ are smooth and continuous at the borders between the regions, and then generalize Eq. (6) along the whole system. In this case, thresholds $\tilde{\xi}^j$ turn into $x$-dependent functions $\tilde{\xi}^j \equiv \tilde{\xi}(x)$, which play the role of potential energy in optical analog of 1D Schröedinger equation Eq. (6):

$$\frac{\partial^2 \tilde{\psi}(x)}{\partial x^2} + [\tilde{E} - \tilde{\xi}(x)] \psi(x) = 0. \qquad (32)$$

Equation (32) possesses no bound state solutions for localized in $y$ direction modes [$\tilde{\xi}(x) < 0$] because $\tilde{E} = q_0^2 > 0$ by definition. The situation can be changed if we use size quantization that is provided by confining wave motion in the $y$ direction by rigid (ideally conducting) walls. As a result, size-quantized thresholds $\tilde{\xi}^j$ and $\tilde{\xi}(x)$ in Eqs. (30), and (32) can become positive and change the sign of the difference $\tilde{E} - \tilde{\xi}(x)$ to form an effective "quantum-mechanical potential barrier." Hence, localized solution of (32) do appear.

Herewith, the role of quantum well in the $x$ direction in Eq. (32) plays the region with waveguide expansion in the $y$ direction giving smaller $\tilde{\xi}(x)$. After these precautions (regarding conditions for bound state existence) have been
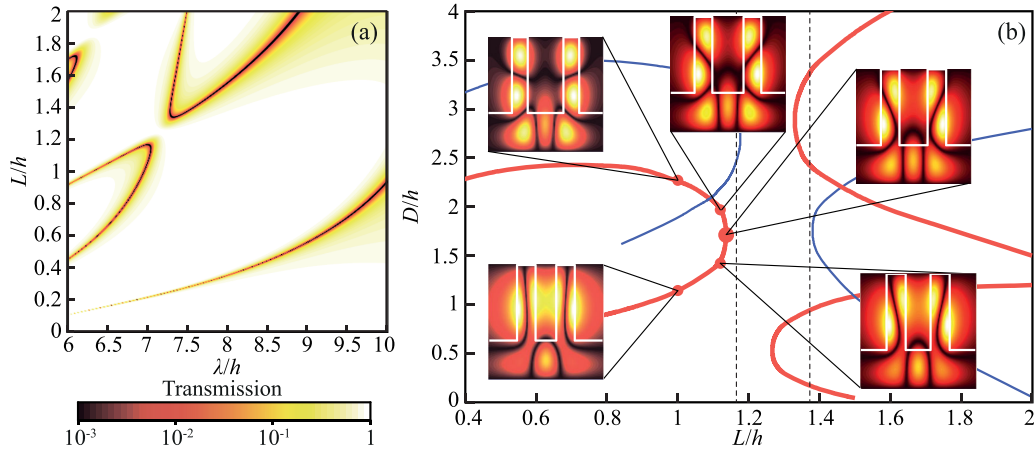
FIG. 13. (a) Numerically calculated wavelength-vs-resonator-length diagrams of the single resonator transmission coefficient for $H = 3h$. (b) Dependence of the distance between the resonators required for BIC formation $D_{\mathrm{BIC}}$ on the length of an individual resonator $L$. Symmetric (thick red lines) and antisymmetric (thin blue lines) BICs demonstrate merging near the points of antiresonance coalescence (black thin dashed lines). Inset in part (b) shows the evolution of the electric field distribution along the 2D structure at BIC during symmetric BIC merging.

taken, practically all qualitative predictions of a quantum-mechanical model are applicable to the electromagnetic one. The difference arises due to some peculiarities mainly related to the explicit dependence of the effective potential $\tilde{U}(x, y)$ on energy $\tilde{E}$ and the presence of the energy dependence of the matrix elements $\mu_{ij}$ between the regions. Nevertheless, we believe that it is instructive to illustrate one of the key results—FP BICs merging due to antiresonance coalescence in optical waveguide as well. The numerical procedure for solving the Helmholtz equation (28) is similar to the procedure for solving the Schrödinger equation (transverse modes decomposition). The key difference is that the parameter $\Delta$ is introduced in the quantum-mechanical problem to simplify the calculation scheme and its value is chosen in accordance with the convergence of the calculation results to the exact solution (corresponding to $\Delta \to \infty$). In the optical problem, however, $\Delta$ (distance between the waveguide and ideally conducting walls) becomes a meaningful physical parameter that provides the size quantization in the $y$ direction, and the calculation results are essentially determined by its particular value. Nevertheless, the qualitative picture of the BIC merging phenomenon remains, and, for simplicity, below we restrict ourselves to the simplest case $\Delta = 0$.

Figure 13(a) depicts the evolution of the transmission spectrum of a 2D optical waveguide with a single expansion (i.e., resonator) with variation of the resonator length $L$. One can see a region of coalescence of antiresonances at $\lambda \sim 7h - 7.5h$ and $L \sim 1.1h - 1.3h$. The behavior of FP BICs in the structure with two such resonators as mirrors (FP resonator) is illustrated in Fig. 13(b). As we expect, BICs demonstrate merging near the coalescence of antiresonances (indicated by thin dashed lines). The larger $D$ is the less influence has evanescent coupling between the resonators, and, hence, the more precisely BICs follow antiresonances. Distribution of the electric field across the structure at BIC changes continuously as one moves along the BIC existence curve in the $D$-$L$ space [Fig. 13(b)] and does not have any abrupt change at the BIC merging point.

## V. CONCLUSION AND DISCUSSION

In our paper, we study interacting bound states in the continuum (BICs), which appeared to become a new and perspective platform for the formation of high- and ultrahigh-$Q$ resonances, which are very desirable for a wide range of applications. We focus on BICs in a finite Fabry-Pérot (FP) resonator structure, which demonstrate complicated mutual interactions and transformations. In particular, such interaction can result in BIC merging and, as we show, repulsion that increases $Q$-factor even further.

The FP resonator structure can possesses two different types of BICs. They are actual FP BICs, formed by trapped wave in the cavity between the mirrors, and recently proposed twin-BICs (TBICs) originating from BICs in individual mirrors of the FP resonator. FP BICs and TBICs are complementary phenomena: while the former weakly depend on mirror parameters and are periodic in FP cavity length the latter possess a weak dependence on the cavity length and a strong one on mirror parameters. The characteristic feature of TBIC is a small wave amplitud inside the cavity, which vanishes in the limit of large cavity lengths. Here we have shown that formation of TBICs is a universal phenomenon related to the sharp dependence of the mirror reflection coefficient phase on the system parameters near the BIC point in the parameter space of an individual mirror. Hence, even if BIC does not exist in a single mirror, it do manifests itself as TBIC in the FP structure. TBIC can be considered as a simplest two-state "BIC molecule." The study of more complex structures will be presented elsewhere.

In waveguides, even a single mirror displays a number of Fano resonances that can interact with each other. Recently, it has been shown [19,35,38] that two perfect antiresonances (with a zero transmission coefficient) can coalesce at some value of the system parameter and transform into one with nonzero transmission under further variation of this parameter. As we show in the present paper, coalescence of the Fano antiresonances provides FP BIC related to these reso-

nances to merge (coalesce or annihilate) as well. However, the interpretation of this physical mechanism of FP BIC merging does not require the introduction of any topological charges, which, for instance, have been discussed in Ref. [37] in the context of experimentally observed FP BICs merging in acoustic resonators. Topological nature of a physical phenomenon assumes its robustness in respect to any smooth variation of system parameters. In our study of BIC interaction in finite resonators, we found out that just the very type of this interaction can be changed by a small parameter variation, and one can observe smooth transformation from merging of BICs over their crossing to avoided crossing (repulsion). The question of the possible existence of topological charges of BICs in finite resonators requires further study. However, taken together the results of our paper indicate that topological properties of BICs in finite resonators, if they really exist, are rather of emerging than fundamental nature and the peculiarities of BIC interaction can be explained without invoking the notion of topological charges.

It is important to note that, in our model, BIC merging results from intrinsic wave interference in the mirrors and, hence, it depends very weak on evanescent coupling between them. This coupling vanishes as the cavity length $D$ increases, while in our model the merging pattern persists for large $D$ as well. Moreover, we show that merging is almost periodic in $D$ with approximate period defined by the FP cavity round-trip phase shift.

We also have shown that a supersharp increase of the $Q$-factor in the vicinity of BIC merging is not specific to the very point of BIC annihilation in the parameter space. It is rather a property of the line in the parameter space, along which evolution of the $Q$-factor is studied. If this line is tangent to the BIC existence curve, then the $Q$-factor blows up sharper in the vicinity of a BIC. In the case of the BIC merging point, the tangent line only becomes parallel to one of the parameters axis making this specific behavior of the $Q$-factor easier to observe and analyze.

In our paper, we focus on BICs in FP resonators as they represent a relatively simple class of systems displaying a rich variety of BIC-related phenomena involving their interaction and transformation. However, we believe that our results are quite general and pave the way for studying new interesting physical objects—complex BIC molecules and arrays of interacting BICs, which may be promising for a variety of applications requiring high-Q resonances.

## ACKNOWLEDGMENT

## APPENDIX A: BOUND STATE IN THE CONTINUUM IN AN ASYMMETRIC RESONATOR WITHIN THE TWO-MODE APPROXIMATION

Consider a single resonator (e.g., waveguide expansion playing the role of a mirror in the FP structure) of length $L$ coupled to two different waveguides (Fig. 14). Within the two-mode approximation, mode mixing on the interface between the resonator and the left/right waveguides is described by
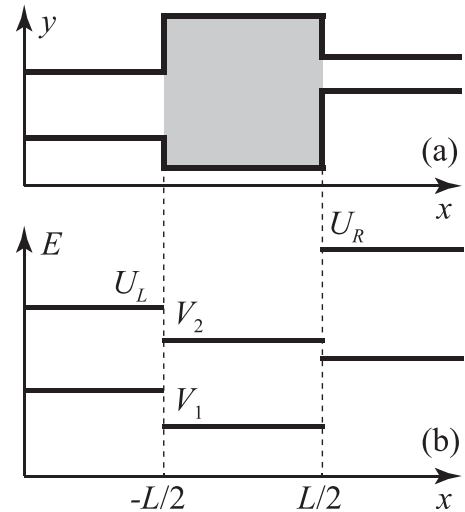


FIG. 14. (a) Schematic view of a 2D resonator (confinement regions) attached to two different waveguides. (b) Thresholds of the transverse modes in the waveguides and inside the resonator within the two-mode approximation.

$2 \times 2$ orthogonal matrices $\hat{\mu}_{L,R}$ correspondingly. We will look for the following form of the longitudinal components of the BIC eigenstate:

$$\psi_1^1(x) = \psi_1^3(x) \equiv 0,$$
$$\psi_2^1(x) = ae^{\kappa_L\left(x+\frac{L}{2}\right)}, \quad \psi_2^3(x) = ce^{-\kappa_R\left(x-\frac{L}{2}\right)},$$
$$\psi_{1,2}^2(x) = b_{1,2}\cos\left[\frac{q_{1,2}}{2}x + \alpha_{1,2}\right]. \tag{A1}$$

Here $\kappa_{L,R} = \sqrt{U_{L,R} - E}$ are decaying coefficients in the evanescent modes of the left (L) and right (R) waveguides, respectively and $q_{1,2} = \sqrt{E - V_{1,2}}$ are the wave numbers in the first and second transverse modes in the resonator.

Applying matching conditions (7), one gets eight equations for four amplitudes $a$, $b_{1,2}$, and $c$. Consistency of this system provides five equations: for phases $\alpha_{1,2}$, energy and resonator length corresponding to BIC, and the specific condition on the coupling matrices $\hat{\mu}_{L,R}$. The first four equations are as follows:

$$\tan\left(\frac{q_{1,2}L}{2} - \alpha_{1,2}\right) = \frac{\kappa_L}{q_{1,2}},$$
$$\tan\left(\frac{q_{1,2}L}{2} + \alpha_{1,2}\right) = \frac{\kappa_R}{q_{1,2}}, \tag{A2}$$

and the last one can be written as

$$\frac{(\mu_L)_{12}/(\mu_L)_{11}}{(\mu_R)_{21}/(\mu_R)_{11}} = \frac{c_1^- c_2^+}{c_1^+ c_2^-} \tag{A3}$$

with $c_{1,2}^{\pm} = \cos\left(\frac{q_{1,2}L}{2} \pm \alpha_{1,2}\right)$. Equations (A2) describe states 2-1-2 and 2-2-2 (localized in the second modes outesude the well and in the first or second mode inside the well, respectively) in the asymmetric quantum well with bottom energy $V_{1,2}$ and left/tight barriers $U_{L,R}$. Simultaneous fulfillment of Eqs. (A2) requires degeneracy of states 2-2-2 and 2-1-2 as it was shown previously in symmetric resonators [35,42,43,51].
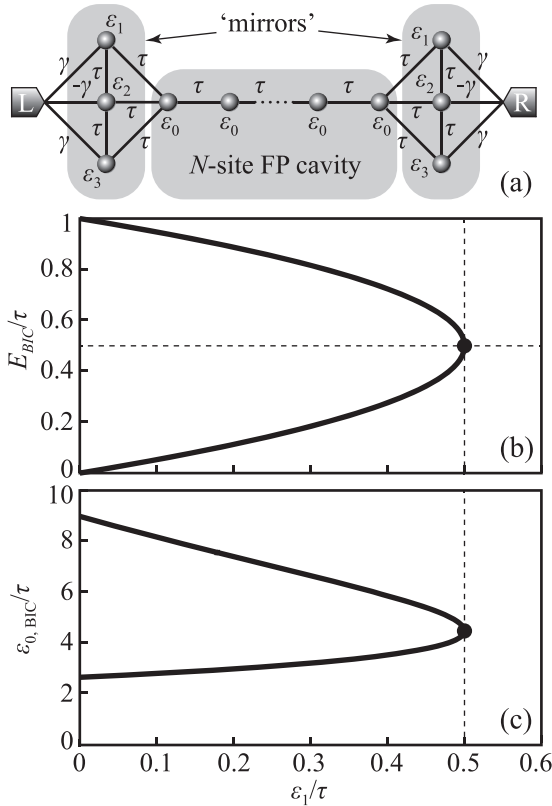
FIG. 15. (a) Tight-binding toy-model of FP resonator with nontrivial mirrors. (b) Dependence of BIC energy $E_{BIC}$ and (c) corresponding energy of the site between the resonators $\varepsilon_{0,BIC}$ on a given value of $\varepsilon_1$ for $\varepsilon_2 = 0.5\tau$. Merging of BICs takes place exactly at the point of antiresonance coalescence in a single resonator at $E = \varepsilon_2$ and $\varepsilon_1 = \varepsilon_2$ (shown by thin dashed black lines).

However, in the case of asymmetric system, there is the additional condition (A3). This requirement can be easily reformulated to the proportionate coupling condition [34]. Indeed, coupling coefficients $\gamma_{1,2}^{L,R}$ between the states of the isolated resonator and the propagating modes in the left/right waveguides are related to matrix elements of $(\hat{\mu}_L)_{1n}$ and $(\hat{\mu}_R)_{n1}$ [52,53]. Here $n = 1$ for 2-1-2 states and $n = 2$ for 2-2-2 states. Using Eqs. (A2) and (A3), one can derive the exact proportionate coupling condition:

$$\frac{\gamma_1^L}{\gamma_2^L} = \frac{\gamma_1^R}{\gamma_2^R}. \tag{A4}$$

## APPENDIX B: GENERIC TIGHT-BINDING TOY-MODEL OF BIC MERGING DUE TO ANTIRESONANCE COALESCENCE

Consider the toy-model shown in Fig. 15(a). The resonators playing role of mirrors are modeled by a three-site block each with the Hamiltonian

$$\hat{H}_{res} = \begin{pmatrix} \varepsilon_1 & \tau & 0 \\ \tau & \varepsilon_2 & \tau \\ 0 & \tau & \varepsilon_3 \end{pmatrix}. \tag{B1}$$

Three is the least needed number of sites in a single resonator to describe the possibility of antiresonance coalescence be-

cause the order of the polynomial function $P(E)$, which is the numerator of the transmission coefficient, is not greater than $M - 1$, where $M$ is the dimensionality of the Hilbert space of the system [19].

Typically, the coalescence of antiresonances takes place in the vicinity of states of opposite parity [38]. Therefore we suppose that individual resonator couples to the left and right waveguides through the following coupling vector between its localized states and the propagating mode of the waveguide:

$$\mathbf{u}_L^{res} = (\gamma, -\gamma, \gamma)^\top, \quad \mathbf{u}_R^{res} = (\gamma, \gamma, \gamma)^\top. \tag{B2}$$

Following formalism of Ref. [19], one can derive from Eqs. (B1) and (B2) the numerator of the single resonator transmission coefficient:

$$P(E) = 2\gamma^2(E^2 - 2E\varepsilon_2 + \varepsilon_1\varepsilon_2). \tag{B3}$$

Here we have set $\varepsilon_3$ as energy origin. Equation (B3) shows that individual resonator has zero transmission at $E = \varepsilon_2 \pm \sqrt{\varepsilon_2(\varepsilon_2 - \varepsilon_1)}$ for $\varepsilon_1 < \varepsilon_2$. Coalescence of antiresonances takes place for $\varepsilon_1 = \varepsilon_2$, and there are no zero transmission dips for $\varepsilon_1 > \varepsilon_2$.

If one places an $N$-site chain as an FP cavity between the mirrors [Fig. 15(a)], then the whole structure will resemble an FP resonator. For simplicity, here we focus on the case $N = 1$, so the Hamiltonian of the whole toy-model structure is

$$\hat{H} = \begin{pmatrix} \hat{H}_{res} & \mathbf{v} & 0 \\ \mathbf{v}^\dagger & \varepsilon_0 & \mathbf{v}^\dagger \\ 0 & \mathbf{v} & \hat{H}_{res} \end{pmatrix}, \tag{B4}$$

where $\mathbf{v} = (\tau, \tau, \tau)^\top$. Coupling of this structure to the waveguides is described by the following vectors:

$$\mathbf{u}_L = (\gamma, -\gamma, \gamma, 0, 0, 0)^\top, \quad \mathbf{u}_L = (0, 0, 0, \gamma, -\gamma, \gamma)^\top. \tag{B5}$$

According to the analysis presented above, we expect BIC merging in the whole structure at $\varepsilon_1 = \varepsilon_2$ with two possible BICs for $\varepsilon_1 < \varepsilon_2$ and no BICs for $\varepsilon_1 > \varepsilon_2$. Indeed, from Eqs. (B4) and (B5), one can derive that BIC in the toy-model structure appears to be for

$$\varepsilon_0 = \varepsilon_2 + \tau - |(\varepsilon_1 - \varepsilon_2)\varepsilon_2 + 5\tau^2| \frac{-\tau\sigma \pm \sqrt{\varepsilon_2(\varepsilon_2 - \varepsilon_1)}}{(\varepsilon_1 - \varepsilon_2)\varepsilon_2 + \tau^2} \tag{B6}$$

with $\sigma = \text{sign}[(\varepsilon_1 - \varepsilon_2)\varepsilon_2 + 5\tau^2]$. Dependence of BIC energy and required energy of the site between the resonators $\varepsilon_0$ is exemplified in Fig. 15. Merging of BICs corresponds exactly to the coalescence of antiresonances in a single resonator at $E = \varepsilon_2$ and $\varepsilon_1 = \varepsilon_2$.

## APPENDIX C: $Q$-FACTOR OF RESONANT STATE NEAR BIC FORMATION CONDITIONS

BIC has an infinite lifetime, i.e., infinite $Q$-factor. A deviation of any system parameter $p$ from its specific value $p_0$ corresponding to the BIC formation results in the transformation of BIC into a decaying resonant state with the finite $Q$-factor (the inverse imaginary part of the effective Hamiltonian eigenvalue) [2,11]

$$Q \sim \Delta p^{-n}, \tag{C1}$$

where $\Delta p = p - p_0$ and $n = 2$. The $Q$-factor of a resonant state near the point of two BIC merging is known for an extra sharp dependence of the $Q$-factor [$n = 4$ in Eq. (C1)] on the parameter detuning from the BIC condition [36,37].

However, BIC merging point is not specific for this property in finite systems. Indeed, suppose that BIC formation condition is fulfilled on a certain curve in a 2D space of some parameters $p_1$ and $p_2$ [e.g., in the example considered in Appendix B, parameters are $\varepsilon_1/\tau$ and $\varepsilon_0/\tau$ and the BIC existence curve is shown in Fig. 15(c)]. Let us take some specific point $(p_1^0, p_2^0)$ on this curve and consider shift of $p_1$ and $p_2$ along the tangent line to the BIC existence curve at this point:

$$(p_1, p_2) = (p_1^0, p_2^0) + \Delta x(a, b). \quad \text{(C2)}$$

Here coefficients $a$ and $b$ are adjusted to make this line a tangent with dimensionless $\Delta x$ being its natural parameter. Being a tangent to the BIC existence curve, line (C2) provides detuning of the parameters from their values required for BIC formation $\Delta p$ to be quadratic in $\Delta x$ [see Fig. 16(a)]. Therefore the $Q$-factor of the resonant state will follow Eq. (C1) with $n = 4$ for parameters shift along the tangent line (C2). Moreover, if the tangent line is drawn at an inflection point of the BIC existence curve then we will have $\Delta p \sim \Delta x^3$ [see Fig. 16(b)] and consequently $Q \sim \Delta x^{-6}$.

For instance, let us consider the example toy-model system from Appendix B. BIC existence curve in the $\varepsilon_1/\tau$ and $\varepsilon_0/\tau$ parameter space is presented in Fig. 15(c). In Fig. 16(c), we reproduce this curve with several different paths of parameter change. Path 1 is a secant line, path 2 is a tangent line at the BIC merging point, path 3 is a tangent line at some other point of the curve, and path 4 is tangent line at the inflection point of the BIC existence curve. Figure 16(c) depicts dependence of the $Q$-factor (inverse imaginary part of the effective Hamiltonian eigenvalue) on the natural parameter of these paths. As expected, the parameters shift along the secant line provides $Q \sim \Delta x^{-2}$, shift along a tangent line results in $Q \sim \Delta x^{-4}$ irrespective to a point, where a tangent line is drawn (whether it is the BIC merging point or not), and finally, the parameters shift along the tangent line drawn at the inflection point gives $Q \sim \Delta x^{-6}$.
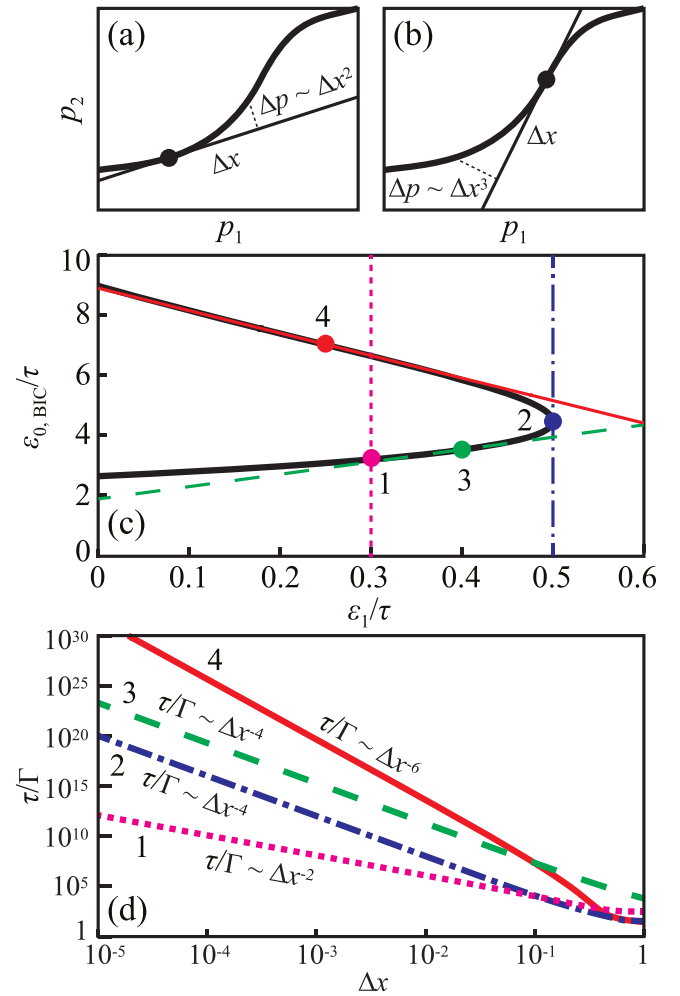


FIG. 16. [(a) and (b)] Schematic view of the BIC existence curve in the $p_1$-$p_2$ parametric space (thick) with tangent lines drawn at some point of general position (a) and at an inflection point (b). (c) BIC existence curve in the space of $\varepsilon_1/\tau$ and $\varepsilon_0/\tau$ parameters of the toy-model system described in Appendix B with four different paths: 1 – line intersecting the curve, 2 – tangent line at the BIC merging point, 3 – tangent line at some point of general position, and 4 – tangent line at an inflection point. (d) Dependence of the $Q$-factor (inverse imaginary part of the effective Hamiltonian eigenvalue) on the natural parameter of the paths in the parameter space shown in part (c).

[1] Z. Liu, Y. Xu, Y. Lin, J. Xiang, T. Feng, Q. Cao, J. Li, S. Lan, and J. Liu, High-q quasibound states in the continuum for nonlinear metasurfaces, Phys. Rev. Lett. **123**, 253901 (2019).

[2] K. Koshelev, S. Lepeshov, M. Liu, A. Bogdanov, and Y. Kivshar, Asymmetric metasurfaces with high-q resonances governed by bound states in the continuum, Phys. Rev. Lett. **121**, 193903 (2018).

[3] X. Zong, L. Li, and Y. Liu, Bound states in the continuum enabling ultra-narrowband perfect absorption, New J. Phys. **25**, 023020 (2023).

[4] I. Deriy, I. Toftul, M. Petrov, and A. Bogdanov, Bound states in the continuum in compact acoustic resonators, Phys. Rev. Lett. **128**, 084301 (2022).

[5] C. W. Hsu, B. Zhen, A. D. Stone, J. D. Joannopoulos, and M. Soljačić, Bound states in the continuum, Nat. Rev. Mater. **1**, 16048 (2016).

[6] K. Koshelev, G. Favraud, A. Bogdanov, Y. Kivshar, and A. Fratalocchi, Nonradiating photonics with resonant dielectric nanostructures, Nanophotonics **8**, 725 (2019).

[7] A. Krasnok, D. Baranov, H. Li, M.-A. Miri, F. Monticone, and A. Alú, Anomalies in light scattering, Adv. Opt. Photon. **11**, 892 (2019).

[8] S. I. Azzam and A. V. Kildishev, Photonic bound states in the continuum: From basics to applications, Adv. Opt. Mater. **9**, 2001469 (2021).

[9] A. F. Sadreev, Interference traps waves in an open system: Bound states in the continuum, Rep. Prog. Phys. **84**, 055901 (2021).

[10] K. L. Koshelev, Z. F. Sadrieva, A. A. Shcherbakov, Y. S. Kivshar, and A. A. Bogdanov, Bound states in the continuum in photonic structures, Usp. Fiz. Nauk **193**, 528 (2023).

[11] H. Friedrich and D. Wintgen, Interfering resonances and bound states in the continuum, Phys. Rev. A **32**, 3231 (1985).

[12] T. V. Shahbazyan and M. E. Raikh, Two-channel resonant tunneling, Phys. Rev. B **49**, 17123 (1994).

[13] C. W. Hsu, B. Zhen, J. Lee, S.-L. Chua, S. G. Johnson, J. D. Joannopoulos, and M. Soljačić, Observation of trapped light within the radiation continuum, Nature (London) **499**, 188 (2013).

[14] B. Zhen, C. W. Hsu, L. Lu, A. D. Stone, and M. Soljačić, Topological Nature of optical bound states in the continuum, Phys. Rev. Lett. **113**, 257401 (2014).

[15] M. S. Sidorenko, O. N. Sergaeva, Z. F. Sadrieva, C. Roques-Carmes, P. S. Muraev, D. N. Maksimov, and A. A. Bogdanov, Observation of an accidental bound state in the continuum in a chain of dielectric disks, Phys. Rev. Appl. **15**, 034041 (2021).

[16] A. E. Miroshnichenko, S. Flach, and Y. S. Kivshar, Fano resonances in nanoscale structures, Rev. Mod. Phys. **82**, 2257 (2010).

[17] C. S. Kim, A. M. Satanin, Y. S. Joe, and R. M. Cosby, Collapse of resonance in quasi-one-dimensional quantum channels, J. Exp. Theor. Phys. **89**, 144 (1999).

[18] E. N. Bulgakov and A. F. Sadreev, Bound states in the continuum in photonic waveguides inspired by defects, Phys. Rev. B **78**, 075105 (2008).

[19] A. A. Gorbatsevich and N. M. Shubin, Unified theory of resonances and bound states in the continuum in hermitian tight-binding models, Phys. Rev. B **96**, 205441 (2017).

[20] M. L. Ladron de Guevara, F. Claro, and P. A. Orellana, Ghost fano resonance in a double quantum dot molecule attached to leads, Phys. Rev. B **67**, 195335 (2003).

[21] L. Yuan and Y. Y. Lu, Strong resonances on periodic arrays of cylinders and optical bistability with weak incident waves, Phys. Rev. A **95**, 023834 (2017).

[22] Z. F. Sadrieva, M. A. Belyakov, M. A. Balezin, P. V. Kapitanova, E. A. Nenasheva, A. F. Sadreev, and A. A. Bogdanov, Experimental observation of a symmetry-protected bound state in the continuum in a chain of dielectric disks, Phys. Rev. A **99**, 053804 (2019).

[23] E. N. Bulgakov and D. N. Maksimov, Topological bound states in the continuum in arrays of dielectric spheres, Phys. Rev. Lett. **118**, 267401 (2017).

[24] S. G. Tikhodeev, A. L. Yablonskii, E. A. Muljarov, N. A. Gippius, and T. Ishihara, Quasiguided modes and optical properties of photonic crystal slabs, Phys. Rev. B **66**, 045102 (2002).

[25] A. S. Kupriianov, Y. Xu, A. Sayanskiy, V. Dmitriev, Y. S. Kivshar, and V. R. Tuz, Metasurface engineering through bound states in the continuum, Phys. Rev. Appl. **12**, 014024 (2019).

[26] M.-S. Hwang, H.-C. Lee, K.-H. Kim, K.-Y. Jeong, S.-H. Kwon, K. Koshelev, Y. Kivshar, and H.-G. Park, Ultralow-threshold laser using super-bound states in the continuum, Nat. Commun. **12**, 4135 (2021).

[27] Y. Guo, M. Xiao, and S. Fan, Topologically protected complete polarization conversion, Phys. Rev. Lett. **119**, 167401 (2017).

[28] E. N. Bulgakov and D. N. Maksimov, Bound states in the continuum and polarization singularities in periodic arrays of dielectric rods, Phys. Rev. A **96**, 063833 (2017).

[29] N. Shubin, V. Kapaev, and A. Gorbatsevich, Twin bics in waveguide fabry-pérot resonator, JETP Lett. **118**, 401 (2023).

[30] J. Jin, X. Yin, L. Ni, M. Soljačić, B. Zhen, and C. Peng, Topologically enabled ultrahigh-q guided resonances robust to out-of-plane scattering, Nature (London) **574**, 501 (2019).

[31] M. Kang, S. Zhang, M. Xiao, and H. Xu, Merging bound states in the continuum at off-high symmetry points, Phys. Rev. Lett. **126**, 117402 (2021).

[32] E. N. Bulgakov and D. N. Maksimov, Light enhancement by quasi-bound states in the continuum in dielectric arrays, Opt. Express **25**, 14134 (2017).

[33] K. Koshelev, S. Kruk, E. Melik-Gaykazyan, J.-H. Choi, A. Bogdanov, H.-G. Park, and Y. Kivshar, Subwavelength dielectric resonators for nonlinear nanophotonics, Science **367**, 288 (2020).

[34] N. M. Shubin, A. V. Friman, V. V. Kapaev, and A. A. Gorbatsevich, Bound states in the continuum in asymmetrical quantum-mechanical and electromagnetic waveguides, Phys. Rev. B **104**, 125414 (2021).

[35] N. M. Shubin, V. V. Kapaev, and A. A. Gorbatsevich, Multi-mode resonances, intermode bound states, and bound states in the continuum in waveguides, Phys. Rev. B **106**, 125425 (2022).

[36] E. Bulgakov, A. Pilipchuk, and A. Sadreev, Desktop laboratory of bound states in the continuum in metallic waveguide with dielectric cavities, Phys. Rev. B **106**, 075304 (2022).

[37] L. Huang, B. Jia, Y. K. Chiang, S. Huang, C. Shen, F. Deng, T. Yang, D. A. Powell, Y. Li, and A. E. Miroshnichenko, Topological supercavity resonances in the finite system, Adv. Sci. **9**, 2200257 (2022).

[38] N. Shubin, A. Emelianov, Y. Uspenskii, and A. Gorbatsevich, Interacting resonances and antiresonances in conjugated hydrocarbons: exceptional points and bound states in the continuum, Phys. Chem. Chem. Phys. **23**, 20854 (2021).

[39] G. Hernández, *Fabry-Perot Interferometers*, Cambridge Studies in Modern Optics Vol. 3 (Cambridge University Press, Cambridge, 1988).

[40] A. F. Sadreev, E. N. Bulgakov, and I. Rotter, Trapping of an electron in the transmission through two quantum dots coupled by a wire, J. Exp. Theor. Phys. Lett. **82**, 498 (2005).

[41] E. N. Bulgakov and A. F. Sadreev, Bound states in photonic fabry-perot resonator comprised of two nonlinear off-channel defects, JETP Lett. **90**, 744 (2010).

[42] C. S. Kim, A. M. Satanin, Y. S. Joe, and R. M. Cosby, Resonant tunneling in a quantum waveguide: Effect of a finite-size attractive impurity, Phys. Rev. B **60**, 10962 (1999).

[43] N. M. Shubin, V. V. Kapaev, and A. A. Gorbatsevich, Bound states in the continuum in a quantum-mechanical waveguide with a subwavelength resonator, JETP Lett. **116**, 205 (2022).

[44] G. N. Henderson, T. K. Gaylord, and E. N. Glytsis, Ballistic electron transport in semiconductor heterostructures and its analogies in electromagnetic propagation in general dielectrics, Proc. IEEE **79**, 1643 (1991).

[45] M. Asada, Y. Miyamoto, and Y. Suematsu, Gain and the threshold of three-dimensional quantum-box lasers, IEEE J. Quantum Electron. **22**, 1915 (1986).

[46] J. Sánchez-Dehesa, J. A. Porto, F. Agulló-Rueda, and F. Meseguer, Electronic energy levels of quantum-well wires, J. Appl. Phys. **73**, 5027 (1993).

[47] A. A. Gorbatsevich and V. V. Kapaev, Waveguide nanoelectronics, Russ. Microelectron **36**, 1 (2007).

[48] N. M. Shubin, Algebraic approach to annihilation and repulsion of bound states in the continuum in finite systems, J. Math. Phys. **64**, 042103 (2023).

[49] Y. Tsuji, R. Hoffmann, R. Movassagh, and S. Datta, Quantum interference in polyenes, J. Chem. Phys. **141**, 224311 (2014),.

[50] J. D. Joannopoulos, S. G. Johnson, J. N. Winn, and R. D. Meade, *Photonic Crystals* (Princeton University Press, 2011).

[51] C. S. Kim, O. N. Roznova, A. M. Satanin, and V. B. Stenberg, Interference of quantum states in electronic waveguides with impurities, J. Exp. Theor. Phys. **94**, 992 (2002).

[52] A. F. Sadreev, E. N. Bulgakov, and I. Rotter, Bound states in the continuum in open quantum billiards with a variable shape, Phys. Rev. B **73**, 235342 (2006).

[53] K. Pichugin, H. Schanz, and P. Seba, Effective coupling for open billiards, Phys. Rev. E **64**, 056227 (2001).